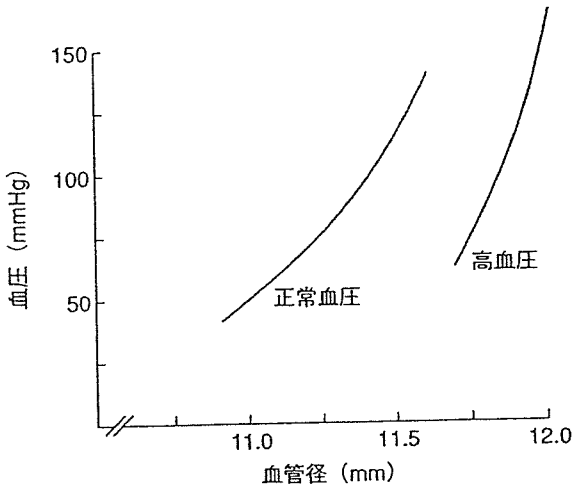


図2 弾性動脈における血管径と血圧の関係
(Nichols WWら，1998[4] より引用)

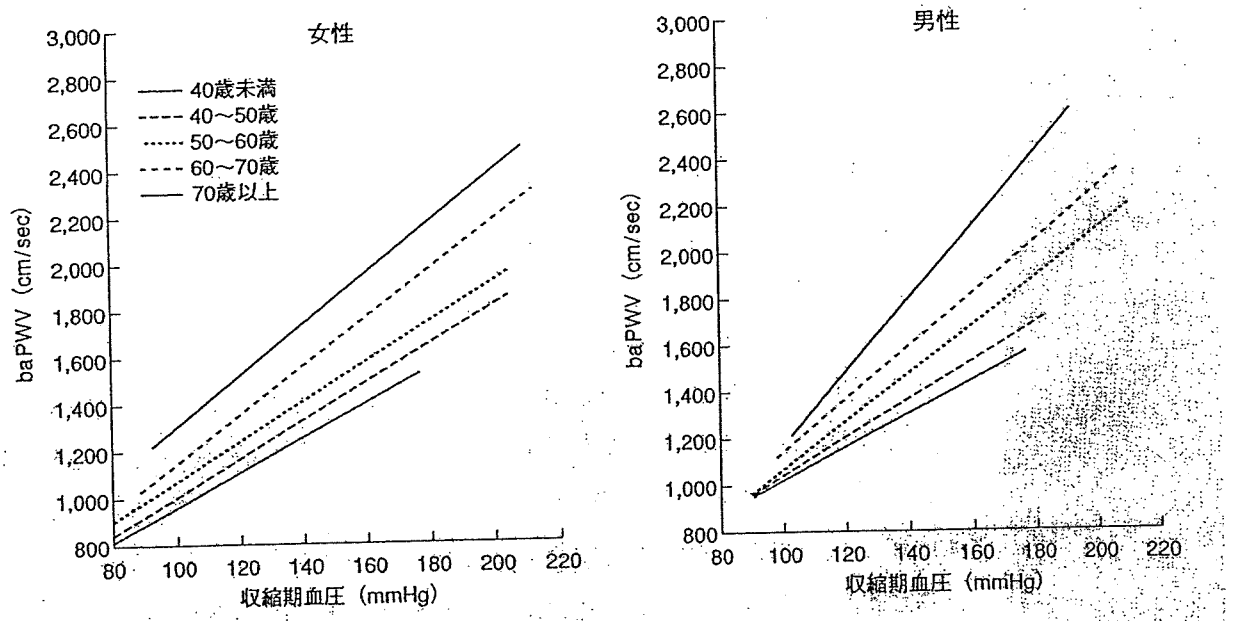


図3 実際の補正式
(東京医科大学，山科章先生の検診データより．コーリンメディカルテクノロジー提供)

## PWVと血圧値に関する報告

PWVが血圧値に影響を受けることについては，いくつかの報告があり，いずれも収縮期血圧値とPWVが有意に関連することを報告している．

Asmarらは18～77歳の男女418例で，頸動脈-大腿動脈PWVと年齢，高血圧の関係を示した．正常血圧群も高血圧群もPWVは収縮期血圧および年齢とともに直線的に上昇し，全例でその関係は次式で示された[5]．

PWV(m/sec)＝0.07×収縮期血圧(mmHg)＋0.09×年齢－4.3

Amarらは地域住民993例を対象に，頸動脈-大腿動脈PWVを計測し，心血管

系疾患危険因子との関連を検討した．高脂血症，糖尿病，高血圧に対する未治療群および治療群で年齢，性別，収縮期血圧がPWVと有意に相関した[6]．

Yamashinaらによる血圧値以外の動脈硬化危険因子を有しない日本人での10,000例を超える検討では，多変量解析の結果，baPWV（上腕動脈-足首動脈PWV）に独立して影響を与えるのは年齢，性別，収縮期血圧値であった[1]．

## 実際の補正

現在広く用いられているform PWV/ABI®（コーリンメディカルテクノロジー）には，東京医科大学山科章先生の検診データをもとにした年齢・性別・血圧での補正式が組み込まれており，年代，血圧値による補正が男女ごとに行われるようになっている[1]（図3）．

## 血圧補正における問題点と注意点

PWVを血圧値で補正するかどうかについては，議論の余地のあるところである．補正をしないでそのままのPWV値を用いることで，血圧，年齢も含めた動脈硬化の指標として用いるという意見がある一方，血圧値で補正して用いるのが有用という意見もある．

また，血圧-PWV特性曲線は，健常者と動脈硬化のリスクを有する疾患群とでは異なることが考えられるので，この曲線を用いて単純に比較してよいかどうかは不明である．実際，高血圧群では血圧に対する血管径の変化もPWV値の増加も健常群と異なることが報告されている[4,5]．補正式においても，上記で用いられているものは直線的な補正のみであり，補正のやり方を変更すれば，拡張期血圧や脈圧で補正できる可能性もある．

さらに問題となるのが，降圧薬による治療前後でPWVを用いて動脈硬化を評価する場合である．降圧薬は短期的に血圧を変化させるが，血圧の変動を除いても降圧薬の種類によりPWVが変化し，血管壁への効果に差を認めるという報告もある．しかし，降圧薬投与後の特性曲線は投薬前と変化している可能性があり，無投薬時の血圧値で補正することが妥当かどうかは不明である．

## 今後の展望

現在のところ，血圧値に対する補正は，横断的な報告をもとにした平均的特性曲線を用いて行われているが，今後，縦断的な研究による特性曲線が求められれば，より正確な補正ができると思われる．また，疾患群別の縦断的研究も待たれる．

（山崎文靖，西永正典，杉浦哲朗，佐藤隆幸）

■文献
1. Yamashina A, et al. Nomogram of the relation of brachial-ankle pulse wave velocity with blood pressure. Hypertens Res 2003；26：801-6.
2. 増田善昭，宮崎　彰．Ⅳ．動脈病変の非観血的診断法　1．中枢および末梢脈波速度．非侵襲的動脈硬化診断研究会編．動脈硬化の診断のガイドライン．東京：共立出版；1999．p.67-75.
3. 入内島十郎．1．脈波の基礎，圧波と血流波：生理学的考察，脈波速度．東京：メジカルビュー社；2002．p.12-6.
4. Nichols WW, O'Rourke MF. McDonald's Blood Flow in Arteries. Theoretical, experimental and clinical principles. 4th ed. London：Arnold；1998. p.379.
5. Asmar R, et al. Assessment of arterial distensibility by automatic pulse wave velocity measurement. Validation and clinical application studies. Hypertension 1995；26：485-90.
6. Amar J, et al. Arterial stiffness and cardiovascular risk factors in a population-based study. J Hypertens 2001；19：381-7.

*J Appl Physiol* 97: 984–990, 2004.
First published May 7, 2004; 10.1152/japplphysiol.00162.2004.

# Bionic epidural stimulation restores arterial pressure regulation during orthostasis

**Yusuke Yanagiya,[1,2] Takayuki Sato,[1,3] Toru Kawada,[1] Masashi Inagaki,[1] Teiji Tatewaki,[1,4] Can Zheng,[1,2] Atsunori Kamiya,[1] Hiroshi Takaki,[1] Masaru Sugimachi,[1] and Kenji Sunagawa[1]**

[1]*Department of Cardiovascular Dynamics, National Cardiovascular Center Research Institute, Suita, Osaka 565-8565;*
[2]*Pharmaceuticals and Medical Devices Agency, Chiyoda-ku, Tokyo 100-0013;*
[3]*Department of Cardiovascular Control, Kochi Medical School, Nankoku, Kochi 783-8505;*
*and* [4]*Japan Association for the Advancement of Medical Equipment, Bunkyo-ku, Tokyo 113-0033, Japan*

Submitted 13 February 2004; accepted in final form 30 April 2004

**Yanagiya, Yusuke, Takayuki Sato, Toru Kawada, Masashi Inagaki, Teiji Tatewaki, Can Zheng, Atsunori Kamiya, Hiroshi Takaki, Masaru Sugimachi, and Kenji Sunagawa.** Bionic epidural stimulation restores arterial pressure regulation during orthostasis. *J Appl Physiol* 97: 984–990, 2004. First published May 7, 2004; 10.1152/japplphysiol.00162.2004.—A bionic baroreflex system (BBS) is a computer-assisted intelligent feedback system to control arterial pressure (AP) for the treatment of baroreflex failure. To apply this system clinically, an appropriate efferent neural (sympathetic vasomotor) interface has to be explored. We examined whether the spinal cord is a candidate site for such interface. In six anesthetized and baroreflex-deafferentiated cats, a multielectrode catheter was inserted into the epidural space to deliver epidural spinal cord stimulation (ESCS). Stepwise changes in ESCS rate revealed a linear correlation between ESCS rate and AP for ESCS rates of 2 pulses/s and above ($r^2$, 0.876–0.979; slope, 14.3 ± 5.8 mmHg·pulses$^{-1}$·s; pressure axis intercept, 35.7 ± 25.9 mmHg). Random changes in ESCS rate with a white noise sequence revealed dynamic transfer function of peripheral effectors. The transfer function resembled a second-order, low-pass filter with a lag time (gain, 16.7 ± 8.3 mmHg·pulses$^{-1}$·s; natural frequency, 0.022 ± 0.007 Hz; damping coefficient, 2.40 ± 1.07; lag time, 1.06 ± 0.41 s). On the basis of the transfer function, we designed an artificial vasomotor center to attenuate hypotension. We evaluated the performance of the BBS against hypotension induced by 60° head-up tilt. In the cats with baroreflex failure, head-up tilt dropped AP by 37 ± 5 mmHg in 5 s and 59 ± 11 mmHg in 30 s. BBS with optimized feedback parameters attenuated hypotension to 21 ± 2 mmHg in 5 s ($P < 0.05$) and 8 ± 4 mmHg in 30 s ($P < 0.05$). These results indicate that ESCS-mediated BBS prevents orthostatic hypotension. Because epidural stimulation is a clinically feasible procedure, this BBS can be applied clinically to combat hypotension associated with various pathophysiologies.

baroreceptors; blood pressure; autonomic nervous system; Shy-Drager syndrome; orthostatic hypotension

THE ARTERIAL BAROREFLEX SYSTEM configures a negative feedback system and reduces arterial pressure (AP) disturbances from external influences (9, 15, 22, 23). Sudden onset of hypotension by orthostatic change occurs as a result of baroreflex failure, despite normal functioning of the cardiovascular system and efferent sympathetic nervous system. This condition is seen in multiple-system atrophy (Shy-Drager syndrome) (21, 22, 30) as well as spinal cord injuries (7, 17). Current treatments, such as salt loading (19, 33), cardiac pacing (1, 14), and pharmacological interventions (2, 3, 12, 20), fail to prevent the orthostatic hypotension. These therapies often result in an unwanted increase in AP in the supine position and neither restore nor reproduce the function of the feedback system that forms the basis of AP control (See DISCUSSION).

Previously, our laboratory developed a bionic baroreflex system (BBS) that substitutes the defective vasomotor center with an artificial controller (i.e., an artificial vasomotor center) to restore the native baroreflex function (24, 26). In these animal studies, the celiac ganglion was exposed by laparotomy and stimulated directly as the efferent neural interface in the BBS. However, for clinical application of the BBS, a less invasive and more stable electrical stimulation method is required.

In the present study, we examined the hypothesis that the spinal cord is a candidate site for the efferent neural interface in our bionic strategy. Epidural spinal cord stimulation (ESCS) has been used for the management of patients with malignant neoplasm, angina pectoris, and peripheral ischemia (6, 29). Stimulating the dorsal part of the spinal cord changes sympathetic nerve activity, AP in animals (11, 32) and heart rate in humans (18). If we can delineate how ESCS affects AP quantitatively, then this may lead to clinical application of the BBS. We studied the feasibility of ESCS-mediated BBS using an animal model of central baroreflex failure.

## MATERIALS AND METHODS

*Study design.* BBS is a negative feedback system and consists of two components: peripheral effectors and the artificial vasomotor center (Fig. 1). Peripheral effectors change AP in response to ESCS. The artificial vasomotor center (controller) determines the ESCS rate in response to changes in AP. Using BBS, we computer programmed the artificial vasomotor center and substituted the defective vasomotor center with an artificial vasomotor center.

For this purpose, we first characterized the static as well as dynamic responses of the peripheral effectors. With this knowledge, we then designed an artificial vasomotor center using simulation to delineate the parameters for obtaining optimal AP response. Finally, we evaluated the performance of the ESCS-mediated BBS in cats during orthostatic AP changes.

*Animals and surgical procedures.* Animals were cared for in strict accordance with the "Guiding Principles for the Care and Use of Animals in the Field of Physiological Sciences," approved by the Physiological Society of Japan. Six adult cats of either sex, weighing

Address for reprint requests and other correspondence: M. Sugimachi, Dept. of Cardiovascular Dynamics, National Cardiovascular Center Research Institute, 5-7-1 Fujishirodai, Suita 565–8565, Japan.

The costs of publication of this article were defrayed in part by the payment of page charges. The article must therefore be hereby marked "*advertisement*" in accordance with 18 U.S.C. Section 1734 solely to indicate this fact.

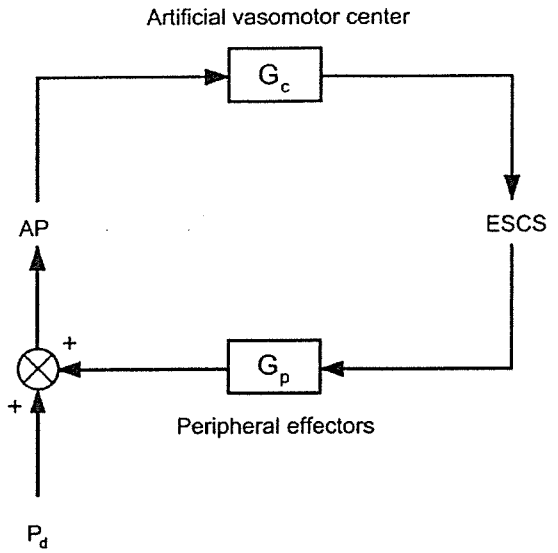


Fig. 1. Simplified diagram of bionic baroreflex system (BBS) using epidural spinal cord stimulation (ESCS). Peripheral effectors change arterial pressure (AP) in response to ESCS. The artificial vasomotor center determines ESCS rate in response to changes in AP. Transfer function of the peripheral effectors ($G_p$) cannot be controlled, but the vasomotor center transfer function ($G_c$) can be computer programmed as needed. $P_d$, pressure disturbance to AP.

1.6–3.7 kg, were premedicated with ketamine (5 mg/kg im) and then anesthetized by intraperitoneal injection (1.0 ml/kg) of a mixture of urethane (250 mg/ml) and α-chloralose (40 mg/ml).

For AP measurement, a high-fidelity pressure transducer (SPC-320, Millar Instruments, Houston, TX) was placed in the aortic arch via the right femoral artery. Pancronium bromide (0.3 mg/kg) was administered to prevent muscular activity. The cats were mechanically ventilated with oxygen-enriched room air. Body temperature was maintained at around 38°C with a heating pad. To produce the baroreflex failure model, the carotid sinus, aortic depressor, and vagal nerves were sectioned bilaterally. The rationale for using baroreceptor-deafferentiated animals as the baroreflex failure model is that, in patients with multiple-system atrophy, the reason for sudden hypotension induced by orthostatic change is a lack of reflex control of AP sensed at the baroreceptors.

A partial laminectomy was performed in the $L_3$ vertebra to expose the dura mater. A multielectrode catheter with interelectrode distance of 10 mm was introduced rostrally ~7 cm into the epidural space. The stimulating electrodes were positioned on the dorsal surface of the spinal cord within $T_{12}$, $T_{13}$, and $L_1$. These spinal levels were selected because our preliminary studies showed that ESCS to these levels produced greater AP response compared with other spinal levels. The catheter was connected to an isolated electric stimulator (SS-102J and SEN7203, Nihon Kohden, Tokyo, Japan) via a custom-made, constant-voltage amplifier. The stimulator was controlled with a laboratory computer (PC9801FA, NEC, Tokyo, Japan).

*Data recording for characterizing AP response to ESCS.* To characterize the static as well as dynamic AP responses to ESCS, we measured AP responses while changing ESCS rate. To estimate static response, we changed the ESCS rate sequentially in stepwise increments and decrements. Each stimulation step was maintained for 90 s. To estimate dynamic response, we randomly changed the ESCS rate, according to a binary white noise sequence with a minimum sequence length of 1 s. In both protocols, the stimulation voltage was fixed at 5 V, and the pulse width of the stimulus was 1 ms. While the stimulation was given, ESCS rate and AP were digitized at a rate of 200 Hz with a 12-bit resolution analog-to-digital converter [AD12–8 (PM), Contec, Osaka, Japan] and stored in another laboratory computer (PC98-NX VA70J, NEC). In this study, "ESCS rate" is defined as the number of stimulation pulses per second and is distinguished from the term "frequency," which refers to how frequently ESCS rate changes.

*Estimation of static AP response parameters.* We parameterized the static AP response to ESCS. Each steady-state AP value was obtained by averaging the AP during the last 10 s of each ESCS step. Stimulation at low-ESCS rate decreased AP, but stimulation at higher rates increased AP. We fit both responses together to a linear regression model of AP vs. ESCS rate. We determined the rate at which the pressor and depressor effects balanced and designated it the offset stimulation rate ($s_o$).

*Estimation of peripheral effector transfer function.* The transfer function of the peripheral effector was estimated by using a white noise method described in detail elsewhere (10, 13, 16, 24–26, 31). Briefly, on the basis of the resampled data at 10 Hz, the linear transfer function from ESCS rate to AP was calculated as a quotient of the ensemble average of cross-power between the two and that of ESCS rate power. The transfer function was calculated up to 0.5 Hz with a resolution of 0.0098 Hz. We parameterized the transfer function by using an iterative, nonlinear, least squares fitting technique (10).

*Design of central characteristics and implementation by the artificial vasomotor center.* Based on the parameterized effector transfer function, we designed the vasomotor center transfer function using computer simulation. The characteristics of the vasomotor center have been identified as derivative characteristics in rabbits and rats (10, 13, 25). We did not have the corresponding data for cats but assumed that they resembled those in rabbits and rats. We adjusted the parameters by simulation, aiming to attenuate hypotension to ~20 mmHg within 5 s and to ≤10 mmHg at 30 s. We implemented designed transfer function by the artificial vasomotor center with convolution algorithm (see APPENDIX).

*Head-up tilt tests.* The efficacy of the BBS against orthostatic stress was evaluated in each animal by the head-up tilt (HUT) test. We placed baroreflex failure animals in a prone position on a custom-made tilt table and measured AP responses to 60° HUT, with or without BBS activation. In the absence of BBS control, we fixed the ESCS rate at $s_o$, irrespective of AP changes. The BBS was activated by sending ESCS command to the stimulator, as calculated by the artificial vasomotor center in response to AP change. Tilt angle, ESCS rate, and AP were stored in a laboratory computer.

*Statistical analysis.* All data are presented as means ± SD. We analyzed AP responses at 5 and 30 s after HUT. AP changes from control value were compared among protocols by using repeated-measures analysis of variance followed by Dunnett's multiple-comparison procedure (8). Differences were considered significant when $P < 0.05$.

## RESULTS

Figure 2*A* is a representative example of static AP response to stepwise ESCS changes. Stepwise increases of ESCS rate produced a depressor response initially at low-ESCS rate and a pressor response at higher rates, and subsequent decreases of ESCS rate produced almost perfect reversal of AP changes. The relationship between AP and ESCS rate appeared nonlinear as a whole (Fig. 2*B*, *top*). However, for ESCS rates of 2 pulses/s and above, there is a linear relationship ($r^2 = 0.964$, AP = 16.0 × ESCS + 44.0, $s_o$ = 3.2 pulses/s; Fig. 2*B*). A linear relationship during ESCS was found in all animals [$r^2$, 0.876–0.979 (median, 0.959) slope, 14.3 ± 5.8 mmHg·pulses$^{-1}$·s; pressure axis intercept, 35.7 ± 25.6 mmHg; $s_o$, 4.9 ± 2.5 pulses/s]. The following protocols were performed by using this linear ESCS range.

Figure 3*A* is a representative example of dynamic AP response to ESCS. We selected low- and high-stimulation rates that produced depressor and pressor responses, respectively,

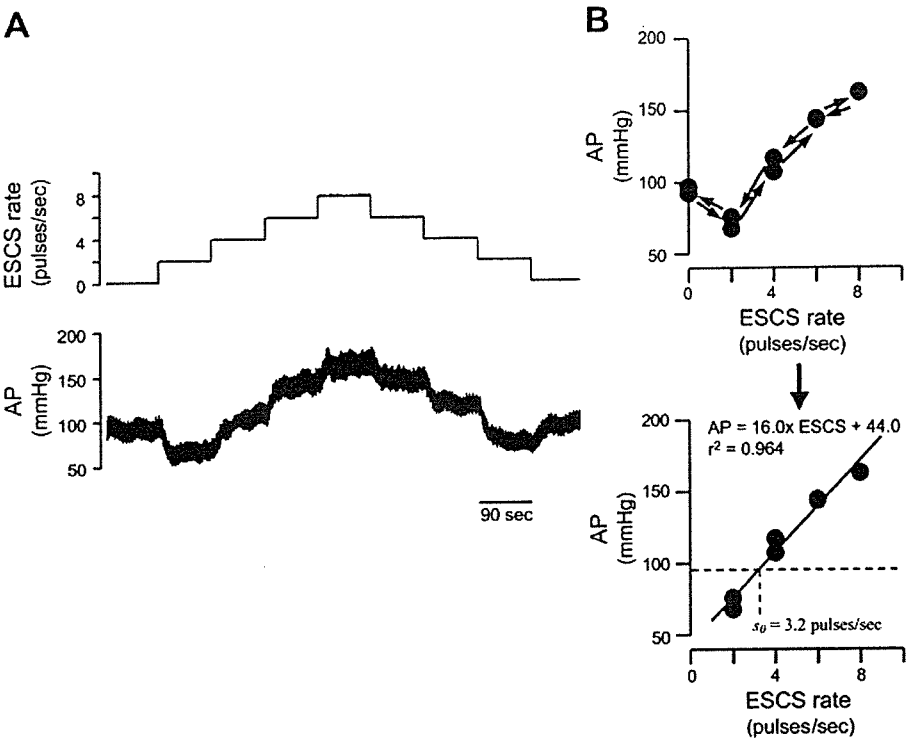


Fig. 2. *A*: representative time series of static AP response to ESCS. Stepwise increases of ESCS rate produced a depressor response initially at low-ESCS rate and a pressor response at higher rates, and subsequent decreases of ESCS rate produced almost perfect reversal of AP changes. *B*: procedures to estimate steady-state relationship between AP and ESCS rate. Each steady-state AP value was plotted against ESCS rate (*top*). Although the relationship between AP and ESCS rate appears nonlinear as a whole, linear regression analysis was conducted for the data obtained during ESCS (2, 4, 6, and 8 Hz), omitting the values before and after ESCS (0 Hz). A linear relationship is obtained. The value $s_o$ represents the stimulation rate where pressor and depressor responses balance.

and stimulated the spinal cord, according to a binary white noise sequence. AP did not respond to fast changes in ESCS rate, but appeared to respond to slower changes, increasing with high-rate stimulation and decreasing with low-rate stimulation. The estimated transfer function indicated low-pass filter characteristics. Figure 3*B* shows the averaged transfer function from ESCS rate to AP in six animals. The gain decreased as the frequency increased and was attenuated to one-tenth of the lowest frequency at 0.1 Hz. The phase approached zero radian at the lowest frequency, reflecting in-phase changes of ESCS rate and AP. The parameters obtained by the least squares fitting to the second-order, low-pass filter model are as follows: dynamic gain = 16.7 ± 8.3 mmHg·pulses$^{-1}$·s, natural frequency = 0.022 ± 0.007 Hz, damping coefficient = 2.40 ± 1.07, and lag time = 1.06 ± 0.41 s. The dynamic gain was much higher than the gain at the lowest frequency in the transfer function (Fig. 3*A*) but comparable to the slope obtained in the static protocol. The coherence function was close to unity between 0.01 and 0.4 Hz, indicating that the input-output relation was governed by almost linear

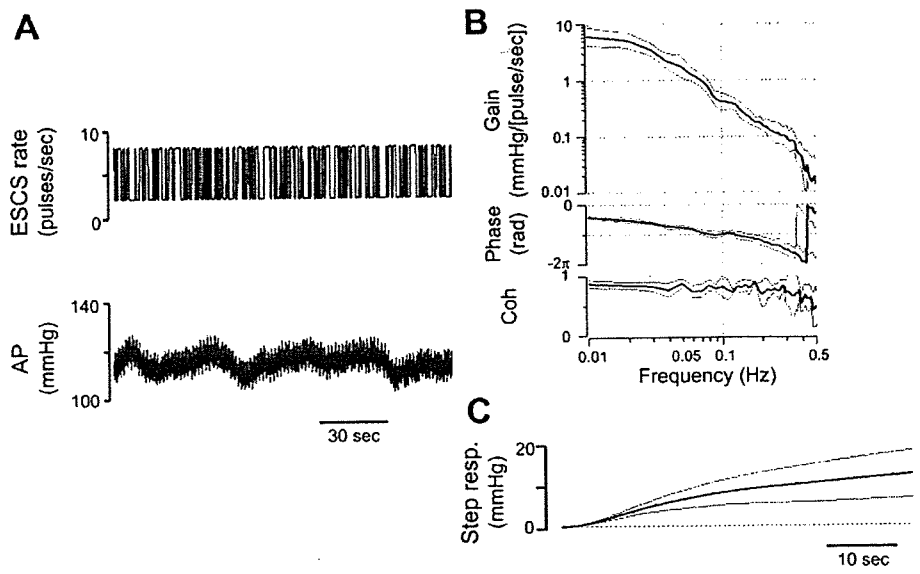


Fig. 3. *A*: representative example of dynamic AP response to ESCS. *B*: averaged transfer functions from ESCS rate to AP, i.e., $G_p$ (gain and phase) and coherence function (Coh). *C*: estimated step response (resp) computed from the transfer function. Data are expressed as means ± SD for 6 cats.

dynamics in this range. To facilitate better understanding of the dynamic AP response to ESCS, the step functions were calculated by time integral of the inverse Fourier transform of the transfer functions. The estimated step functions are averaged and shown in Fig. 3*C*. An initial time lag and overdamped slow AP response to unit step ESCS are evident. The time courses of the estimated step functions were almost identical to but smoother than those of the actually observed AP responses to stepwise ESCS changes, indicating the ability to cancel out noises by the white noise method.

Figure 4 is a representative example of how we designed the vasomotor center transfer function. The steady-state gain is determined simply to match a total baroreflex loop gain of 5. This setting ensures that the steady-state AP fall will be attenuated to 10 mmHg in the case of a depressor stimulus of 60 mmHg. By changing the derivative corner frequency ($f_c$), we simulated various transient AP responses to orthostatic depressor stimulation. Lower $f_c$ causes unstable oscillation in AP (Fig. 4*B*, *left*), and higher $f_c$ slows AP restoration (Fig. 4*B*, *right*). On the basis of these simulations, $f_c$ = 0.02 Hz was selected in this example (Fig. 4*B*, *middle*, 0.018 ± 0.008 Hz in 6 cats).

Figure 5 shows a representative example of real-time application of BBS to a cat. In the control cat with baroreflex failure, abrupt HUT produced a rapid and then progressive fall in AP by 44 mmHg in 30 s (Fig. 5, *left*). Activation of the simulation-based BBS attenuated the AP fall (Fig. 5, *middle*; AP fall, 25 mmHg in 5 s and 19 mmHg in 30 s) but did not attain the predetermined target (gaps indicated by vertical bars in Fig. 5, *middle* and *right*). If the total loop gain of 5 were preserved, the AP fall should theoretically be attenuated to 44/(1 + 5), or ~7 mmHg, according to the linear control theory. The observed attenuation of 19/44 (=1/2.3) indicated that the actual gain was 1.3 (1 + 1.3 = 2.3). To achieve a total loop gain of 5, we increased the gain of the vasomotor center transfer function by 3.8-fold and reassessed the efficacy of BBS. As a result, AP returned to the predetermined target (Fig. 5, *right*; AP fall, 19 mmHg in 5 s, 7 mmHg in 30 s).

Figure 6 summarizes the results obtained from six cats, demonstrating the effectiveness of the BBS performance. In the cat model of baroreflex failure, HUT decreased AP by 37 ± 5 mmHg in 5 s and by 59 ± 11 mmHg in 30 s. In animals with simulation-based vasomotor center, the initial attenuation (AP fall: 32 ± 7 mmHg in 5 s) was not significant, and the steady-state attenuation (17 ± 8 mmHg in 30 s) did not satisfy the predetermined target. On the other hand, in animals with gain-adjusted vasomotor center (2.4 ± 1.1-fold increase), the BBS achieved both initial and the steady-state targets (21 ± 2 mmHg in 5 s, $P < 0.05$; 8 ± 4 mmHg in 30 s, $P < 0.05$).

## DISCUSSION

The present results indicate that AP can be controlled by ESCS and that ESCS-mediated BBS prevents orthostatic hypotension in anesthetized cats. Although the BBS based on simulation alone did not work as predicted during HUT, gain adjustments of the vasomotor center achieved quick and stable restoration of AP.

*Necessity of BBS for treatment of central baroreflex failure.* Conventional treatments for central baroreflex failure aim at increasing AP. Although they alleviate the hypotension to the extent of preventing syncope, they have adverse effects of causing supine hypertension and enhancing the risk of hypertensive organ disease. Recently, Shannon et al. (28) suggested well-timed water consumption as a treatment for orthostatic hypotension in patients with autonomic failure. Their strategy is superior to conventional treatments because it prevents AP fall if predicted in advance. However, at least a few minutes are necessary for their method to increase AP. This time lag makes it impossible to control AP against sudden or unpredictable AP

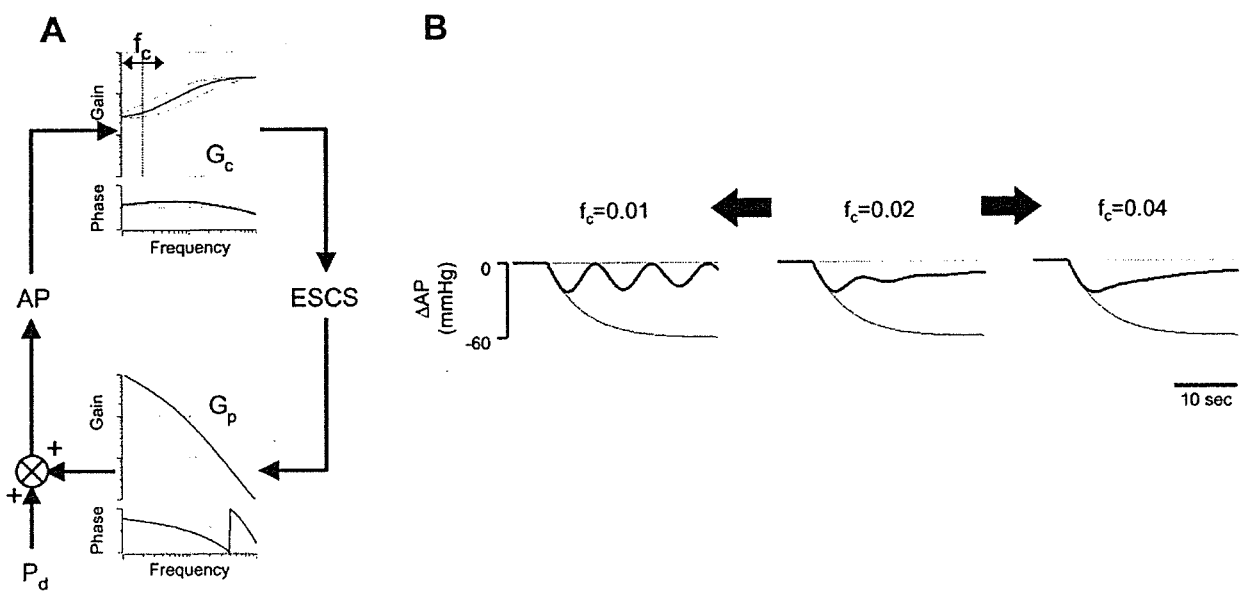


Fig. 4. Representative example of designing the $G_c$. *A*: schematic diagram of the method of designing the $G_c$. AP changes in the presence of $P_d$ were simulated by changing the corner frequency ($f_c$) for derivative characteristic in the $G_c$. *B*: simulation results of this example. A vasomotor center with $f_c$ of 0.02 Hz restores AP with sufficient speed and stability (center).

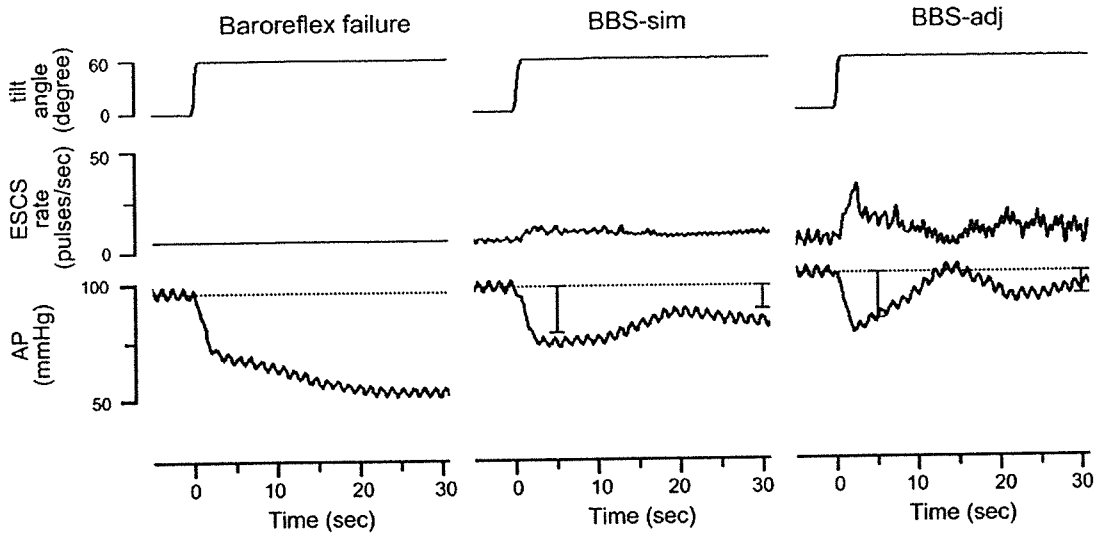


Fig. 5. Representative example of real-time application of the BBS during head-up tilt (HUT). *Left*: in the cat with baroreflex failure, ESCS rate was fixed at 5.0 pulse/s. HUT produced a rapid and then progressive fall in AP. *Middle*: simulation-based BBS (BBS-sim) attenuated the AP fall but did not attain the predetermined target. *Right*: gain adjustment of the vasomotor center (BBS-adj) resulted in quick and sufficient attenuation of AP fall (see text for detail). Vertical bars indicate the ranges of predetermined targets.

fall. None of the treatments attempted so far can prevent sudden orthostatic hypotension because the dynamics of the baroreflex remain impaired.

In contrast, the BBS continuously monitors and controls AP to achieve quick restoration of AP. Because AP is increased via sympathetic pathways, the AP response to the BBS vasomotor center command is as fast as that to the native vasomotor center control. Therefore, the quick, adequate, and stable nature of the native baroreflex system can be restored by the BBS with appropriate settings of the artificial vasomotor center.

*Designing the vasomotor center transfer function and parameter adjustments.* In a negative feedback system, closed-loop responses to external perturbation are dependent on the dynamic characteristics of the total open-loop transfer function. We assumed that the derivative characteristics in cats are identical to those in rabbits or rats, which have been delineated previously (10, 13, 25). We optimized gain and derivative parameters for each cat so that both speed and stability were achieved.

In animal experiments, however, the simulation results were not fully reproduced. Gain adjustments of the vasomotor center were necessary to attain quick and sufficient attenuation of the AP fall. This discrepancy cannot be explained without considering a possible slope decrease or nonlinearity in peripheral effector characteristics (AP-ESCS relationship) caused by the HUT, or both. Pooling of blood volume in the splanchnic and hindlimb circulation would be a cause for such attenuated AP response. If AP responses during posture change can be de-

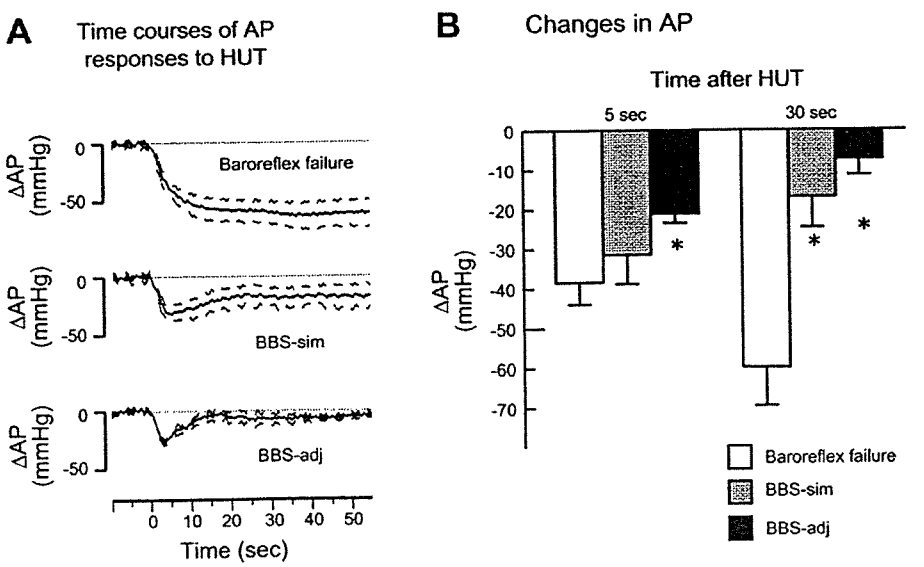


Fig. 6. Summarized results of HUT obtained from 6 cats. *A*: averaged time courses of AP responses to HUT in cats with baroreflex failure (*top*) and with BBS (*middle* and *bottom*). Using the parameters determined from simulation, we found that the BBS (BBS-sim) did not adequately attenuate hypotension in all cats (*middle*). Appropriate gain increase (BBS-adj) was necessary for quick and sufficient attenuation of hypotension (*bottom*). *B*: changes in AP produced by HUT. Data are expressed as means ± SD. $^*P < 0.05$ compared with baroreflex failure.

fined quantitatively, then a more elaborate artificial vasomotor center can be developed that automatically adjusts the parameters. Automated adjustments may also be accomplished with adaptive control systems that execute real-time system identification and self-tuning of controller. The present study suggests the necessity of such manipulation of the vasomotor center settings.

*Pressor and depressor responses by ESCS.* We demonstrated both depressor and pressor responses in AP to ESCS with a linear range (Fig. 2). Earlier studies have shown that dorsal column stimulation produces pressor and depressor responses. Depressor response is produced by a group of dorsal column fibers that project to the dorsal nuclei at the level of $C_8$ to $L_1$ and transmit to the fibers that ascend through the dorsal spinocerebeller tracts (4, 27, 32). Pressor response is produced by another group of fibers that ascends or descends through the terminal zone and enter the gray matter. Some of these fibers project to the intermedial lateral columns to activate sympathetic presynaptic fibers. AP responses to ESCS observed in the present study are the results of compound responses in these multiple pathways. Nevertheless, controllability of AP by the BBS is ascertained by a clear linearity between ESCS and AP response in both static and dynamic relationships.

Although we have not confirmed it in the closed-loop condition, depressor response shown in the open-loop condition indicates that ESCS-mediated BBS can attenuate hypertension as well as hypotension. Because an offset ESCS rate ($s_o$) is applied in the absence of pressure disturbance, lowering ESCS rate would attenuate hypertension to some extent. AP in conscious animals fluctuates between hypertension and hypotension, even in a quiet position (5). The speed of AP restoration is considered sufficient to control these fluctuations.

*Future step for clinical application.* Clearly, the next step toward clinical application is to demonstrate the safety and the effectiveness of the ESCS-mediated BBS during orthostasis in conscious patients and animals. To study BBS in conscious animals, we have been developing an implantable hardware that enables BBS. Elaboration of such devices is mandatory for its future clinical application by searching the optimal stimulating site and condition that do not cause uncomfortable sensation and muscle twitch. A control algorithm must be developed that overcomes the problem revealed in the present study. The developing implant would be as small and low power as a pacemaker, with the aid of recent LSI technologies, and would be telemetrically programmable. In parallel, we began collaboration with a clinical group to develop ESCS-mediated BBS to suppress sudden hypotension in anesthetized humans during surgery. This study would prove the feasibility of human BBS.

Finally, new methods for long-term manometry are definitely required. Intravascular manometry can be achieved only with long-lasting antithrombotic material. Other indirect methods should be used until we are confident in antithrombotic ability.

*Conclusions.* As a step toward clinical application of BBS, we demonstrated that AP could be controlled with ESCS. We designed the artificial vasomotor center based on the dynamic characteristics of AP response to ESCS. Although there was a dissociation between the predicted and actual attenuation of AP fall, ESCS-mediated BBS with appropriate gain adjustment was capable of preventing HUT-induced hypotension rapidly, sufficiently, and stably.

## APPENDIX

### *Simulation of AP Restoration and Implementation by the Artificial Vasomotor Center*

We modeled the vasomotor center transfer function ($G_c$) as

$$G_c(f) = K_c \frac{1 + \frac{f}{f_{c1}}j}{\left(1 + \frac{f}{f_{c2}}j\right)\left(1 + \frac{f}{f_{c3}}j\right)} \exp(-2\pi f j L_c) \qquad (A1)$$

where $f$ is frequency, $K_c$ is the steady-state gain of the artificial vasomotor center, $f_{c1}$ is $f_c$ for derivative characteristics, $f_{c2}$ and $f_{c3}$ are corner frequencies for high-cut characteristics, $j$ is an imaginary unit, and $L_c$ is a pure delay. The value $f_{c2}$ was set to $10 \times f_{c1}$, and $f_{c3}$ was set to 1 Hz. These settings attenuate AP pulsation and preserve total baroreflex gain (13). $L_c$ was introduced to simulate the possible time delay of 0.1 s in transforming AP to ESCS rate but was excluded in real-time application to improve AP stability.

The simulation was performed as follows. The block diagram in Fig. 4*A* is represented as

$$AP = G_p \cdot ESCS + P_d$$

$$ESCS = G_c \cdot AP$$

where $G_p$ is transfer function of the peripheral effectors, and $P_d$ is pressure disturbance to AP. Rearranging these formula yields

$$AP = G_c \cdot G_p \cdot AP + P_d \qquad (A2)$$

The time domain representation of *Eq. A2* is

$$\Delta AP(t) = \int g(\tau) \cdot \Delta AP(t - \tau)d\tau + P_d(t) \qquad (A3)$$

where $\Delta AP(t)$ is AP change from control value, and $g(\tau)$ is the impulse response function of the total open-loop transfer function ($G_c \cdot G_p$). To simulate orthostatic hypotension, $P_d(t)$ is set as an exponential AP fall to $-60$ mmHg with a time constant of 5 s rather than a stepwise fall (see Fig. 6*A*, *top*). We simulated the transient AP response to depressor stimulus while changing $f_{c1}$ in the presence of the negative feedback system.

To implement the designed vasomotor center transfer function, we programmed the artificial vasomotor center to calculate ESCS rate in response to AP changes, according to the following equation:

$$ESCS(t) = \int h(\tau) \cdot \Delta AP(t - \tau)d\tau + s_o$$

where $h(\tau)$ is the impulse response function of the designed vasomotor center transfer function, $\Delta AP(t)$ is AP change from the control value, and $s_o$ is the offset ESCS rate obtained from the static parameterization.

## GRANTS

This study was supported by a Grant-in-Aid for Scientific Research (A15200040) from the Japan Society for the Promotion of Science, the Program for Promotion of Fundamental Studies in Health Science of Pharmaceuticals and Medical Devices Agency of Japan, and a Health and Labour Sciences Research Grant (Research on Advanced Medical Technology, H14-nano-002) from the Ministry of Health, Labour and Welfare of Japan.

## REFERENCES

1. **Bannister R, da Costa DF, Hendry WG, Jacobs J, and Mathias CJ.** Atrial demand pacing to protect against vagal overactivity in sympathetic autonomic neuropathy. *Brain* 109: 345–356, 1986.

2. **Biaggioni I, Robertson RM, and Robertson D.** Manipulation of norepinephrine metabolism with yohimbine in the treatment of autonomic failure. *J Clin Pharmacol* 34: 418–423, 1994.
3. **Chobanian AV, Volicer L, Tifft CP, Gavras H, Liang CS, and Faxon D.** Mineralocorticoid-induced hypertension in patients with orthostatic hypotension. *N Engl J Med* 301: 68–73, 1994.
4. **Chung JM and Wurster RD.** Ascending pressor and depressor pathways in the cat spinal cord. *Am J Physiol* 231: 786–792, 1976.
5. **Cowley AW Jr, Liard JF, and Guyton AC.** Role of baroreceptor reflex in daily control of arterial blood pressure and other variables in dogs. *Circ Res* 32: 564–576, 1973.
6. **Di Pede F, Lanza GA, Zuin G, Alfieri O, Rapati M, Romano M, Circo A, Cardano P, Bellocci F, Santini M, and Maseri A; Investigators of the Prospective Italian Registry of SCS for Angina Pectoris.** Immediate and long-term clinical outcome after spinal cord stimulation for refractory stable angina pectoris. *Am J Cardiol* 91: 951–955, 2003.
7. **Frankel HL and Mathias CJ.** Severe hypertension in patients with high spinal cord lesions undergoing electro-ejaculation–management with prostaglandin E2. *Paraplegia* 18: 293–299, 1980.
8. **Glantz SA.** *Primer of Biostatistics* (4th ed.). New York: McGraw-Hill, 1997.
9. **Guyton AC, Coleman TG, and Granger HJ.** Circulation: overall regulation. *Annu Rev Physiol* 34: 13–46, 1972.
10. **Ikeda Y, Kawada T, Sugimachi M, Kawaguchi O, Shishido T, Sato T, Miyano H, Matsuura W, Alexander J Jr, and Sunagawa K.** Neural arc of baroreflex optimizes dynamic pressure regulation in achieving both stability and quickness. *Am J Physiol Heart Circ Physiol* 271: H882–H890, 1996.
11. **Illert M and Gabriel M.** Descending pathways in the cervical cord of cats affecting blood pressure and sympathetic activity. *Pflügers Arch* 335: 109–124, 1972.
12. **Kachi T, Iwase S, Mano T, Saito M, Kunimoto M, and Sobue I.** Effect of L-threo-3,4-dihydroxyphenylserine on muscle sympathetic nerve activities in Shy-Drager syndrome. *Neurology* 38: 1091–1094, 1988.
13. **Kawada T, Zheng C, Yanagiya Y, Uemura K, Miyamoto T, Inagaki M, Shishido T, Sugimachi M, and Sunagawa K.** High-cut characteristics of the baroreflex neural arc preserve baroreflex gain against pulsatile pressure. *Am J Physiol Heart Circ Physiol* 282: H1149–H1156, 2002.
14. **Kristinsson A.** Programmed atrial pacing for orthostatic hypotension. *Acta Med Scand* 214: 79–83, 1983.
15. **Malliani A, Pagani M, Lombardi F, and Cerutti S.** Cardiovascular neural regulation explored in the frequency domain. *Circulation* 84: 482–492, 1991.
16. **Marmarelis PZ and Marmarelis VZ.** *Analysis of Physiological Systems: The White-Noise Approach.* New York: Plenum, 1978.
17. **Matthews JM, Wheeler GD, Burnham RS, Malone LA, and Steadward RD.** The effects of surface anaesthesia on the autonomic dysreflexia response during functional electrical stimulation. *Spinal Cord* 35: 647–651, 1997.
18. **Meglio M, Cioni B, Rossi GF, Sandric S, and Santarelli P.** Spinal cord stimulation affects the central mechanisms of regulation of heart rate. *Appl Neurophysiol* 49: 139–146, 1986.
19. **Mehlsen J and Boesen F.** Substantial effect of acute hydration on blood pressure in patients with autonomic failure. *Clin Physiol* 7: 243–246, 1987.
20. **Obara A, Yamashita H, Onodera S, Yahara O, Honda H, and Hasebe N.** Effect of xamoterol in Shy-Drager syndrome. *Circulation* 85: 606–611, 1992.
21. **Parikh SM, Diedrich A, Biaggioni I, and Robertson D.** The nature of the autonomic dysfunction in multiple system atrophy. *J Neurol Sci* 200: 1–10, 2002.
22. **Robertson D.** Diagnosis and management of baroreflex failure. *Primary Cardiol* 21: 37–40, 1995.
23. **Sato T, Kawada T, Inagaki M, Shishido T, Takaki H, Sugimachi M, and Sunagawa K.** New analytic framework for understanding sympathetic baroreflex control of arterial pressure. *Am J Physiol Heart Circ Physiol* 276: H2251–H2261, 1999.
24. **Sato T, Kawada T, Shishido T, Sugimachi M, Alexander J Jr, and Sunagawa K.** Novel therapeutic strategy against central baroreflex failure: a bionic baroreflex system. *Circulation* 100: 299–304, 1999.
25. **Sato T, Kawada T, Inagaki M, Shishido T, Sugimachi M, and Sunagawa K.** Dynamics of sympathetic baroreflex control of arterial pressure in rats. *Am J Physiol Regul Integr Comp Physiol* 285: R262–R270, 2003.
26. **Sato T, Kawada T, Sugimachi M, and Sunagawa K.** Bionic technology revitalizes native baroreflex function in rats with baroreflex failure. *Circulation* 106: 730–734, 2002.
27. **Schramm LP and Livingston RH.** Inhibition of renal nerve sympathetic activity by spinal stimulation in rat. *Am J Physiol Regul Integr Comp Physiol* 252: R514–R525, 1987.
28. **Shannon JR, Diedrich A, Biaggioni I, Tank J, Robertson RM, Robertson D, and Jordan J.** Water drinking as a treatment for orthostatic syndromes. *Am J Med* 112: 355–360, 2002.
29. **Shimoji K, Hokari T, Kano T, Tomita M, Kimura R, Watanabe S, Endoh H, Fukuda S, Fujiwara N, and Aida S.** Management of intractable pain with percutaneous epidural spinal cord stimulation: differences in pain-relieving effects among diseases and sites of pain. *Anesth Analg* 77: 110–116, 1993.
30. **Shy M and Drager GA.** A neurological syndrome associated with orthostatic hypotension: a clinico-pathologic study. *Arch Neurol* 2: 511–527, 1960.
31. **Sugimachi M, Imaizumi T, Sunagawa K, Hirooka Y, Todaka K, Takeshita A, and Nakamura M.** A new method to identify dynamic transduction properties of aortic baroreceptors. *Am J Physiol Heart Circ Physiol* 258: H887–H895, 1990.
32. **Taylor RF and Schramm LP.** Spinally mediated inhibition of abdominal and lumbar sympathetic activities. *Am J Physiol Regul Integr Comp Physiol* 254: R655–R658, 1988.
33. **Wilcox CS, Puritz R, Lightman SL, Bannister R, and Aminoff MJ.** Plasma volume regulation in patients with progressive autonomic failure during changes in salt intake or posture. *J Lab Clin Med* 104: 331–339, 1984.

# Effect of Electrical Modification of Cardiomyocytes on Transcriptional Activity through 5′-AMP-activated Protein Kinase

*Yoshihiko Kakinuma*, Yanan Zhang†, Motonori Ando*, Tetsuro Sugiura†, and Takayuki Sato**

**Abstract:** Endothelin-1 (ET-1) is known as an aggravating factor of the failing cardiomyocytes and, therefore, a therapeutic method is indispensable to decrease cardiac ET-1 expression. To study the mechanisms of how cardiac ET-1 gene expression can be modified, we investigated the effect of electrical stimulation against cardiomyocytes. Considering the physiology of cardiomyocytes, in vitro cultured cardiomyocytes demonstrate distinctive features from in vivo cardiomyocytes (i.e. the absence of a stretch along with electrical stimulation). In this study, we especially focused on the effect of electrical stimulation. The electrical stimulation reduced the gene expression of ET-1 mRNA in rat primary cultured cardiomyocytes. Furthermore, this effect on the transcriptional modification of ET-1 was also identified in H9c2 cells. Luciferase activity using H9c2 cells was decreased by electrical stimulation in the early phase, suggesting that the attenuation of the ET-1 gene transcription by electrical stimulation should be due to a transcriptional repression. To further investigate a trigger signal involved in the transcriptional repression, phosphorylation of 5′-AMP-activated protein kinase (AMPK) was evaluated. It was revealed that AMPK was phosphorylated in the early phase of electrical stimulation of H9c2 cells as well as in rat primary cultured cardiomyocytes, and that AMPK phosphorylation was followed by ET-1 transcriptional repression, suggesting that electrical stimulation directly regulates AMPK. This study suggests that AMPK activation in cardiomyocytes plays a crucial role in the transcriptional repression of ET-1.

**Key Words:** endothelin-1, cardiomyocytes, 5′-AMP-activated protein kinase

(*J Cardiovasc Pharmacol*™ 2004;44(suppl 1):S435–S438)

The endothelin (ET) system is known to be indispensable for the development of the heart. In the developmental stage, ET-1 exerts the formation of the heart through the receptors endothelin-A and endothelin-B, and the system exerts the biological function through either autocrine or paracrine fashion. It has been reported that deformity of the heart is produced in the absence of the ET system. Especially, cardiomyocytes have been reported to remarkably express and produce ET-1 in the pathophysiological condition (i.e. the failing heart) compared with the normal heart.[1] The mechanisms have been extensively studied of how the failing heart expresses ET-1 in the progression of heart failure; however, our previous study clearly demonstrated one aspect of the mechanisms — impaired cardiac energy metabolism.[2] The level of cardiac ET-1 gene expression is dependent on the condition of the cardiomyocytes in vivo; the failing cardiomyocytes produce more ET-1. However, even normal primary cultured cardiomyocytes in vitro could extraordinarily express ET-1 compared with in vivo. The abnormal pattern of cardiac ET-1 gene expression in vitro is also accompanied with a surprising switch of the myosin heavy chain isoform from α to β (a fetal pattern), suggesting that our cultured cardiomyocytes have already biologically changed their character.[3] However, this finding might provide us with some therapeutic clue as to how cardiac ET-1 expression can be depressed using cultured cardiomyocytes. If we could obtain some tool to repress cardiac ET-1 gene expression in vitro, it might lead to clarification of one of the therapeutic strategies against heart failure. Consequently we have so far concentrated on searching for ways to decrease cardiac ET-1 gene expression. Among them, we have found several methods to modify the expression using not chemicals or drugs, but physical stimulation.[3] In this study, using electrical stimulation (ES) we have successfully inhibited the cardiac ET-1 gene expression, and investigated the mechanisms by which such stimulation causes a depression of the gene expression.

## METHODS

### Cell Culture of Rat Cardiomyocytes and H9c2 Cells

According to our previous studies,[1] cardiomyocytes were isolated from 2-day-old Wistar–Kyoto rats. 5-Aminoimidazole-4-carboxamide-1-β-D-ribofuranosyl 5-monophosphate (AICAR) was purchased from Sigma (St Louis, MO, U.S.A.), and H9c2 cells were transiently treated by AICAR.

*Department of Cardiovascular Control and †Department of Laboratory Medicine, Kochi Medical School, Nankoku, Kochi, Japan

Address correspondence and reprint requests to Yoshihiko Kakinuma, Department of Cardiovascular Control, Kochi Medical School, Kohasu, Nankoku-shi, Kochi-ken 783-8505, Japan. E-mail: kakinuma@med.kochi-u.ac.jp

This study was supported by a Health and Labor Sciences Research Grant (H14-NANO-002) for Advanced Medical Technology from the Ministry of Health, Labor, and Welfare of Japan.

## Electrical Stimulation

We have developed a specific ES device, which is modified to simultaneously provide multi-channels of ES and also to efficiently regulate bidirectional current. Our protocol for ES was performed as follows: 10 V, 10 milliseconds of duration and 4 Hz of frequency.

## RNA Isolation and Reverse Transcription-Polymerase Chain Reaction

As previously described, total RNA was isolated, and 1 μg total RNA was reverse-transcribed and used for a polymerase chain reaction (PCR) template. PCR primers were prepared for preproET-1, hypoxia-inducible factor (HIF)-1α, β-actin,[2,3] and glucose transporter 3.

## Luciferase Assay

As previously reported, the 5′-regulatory region of preproET-1 gene was subcloned into a luciferase vector.[2] The reporter vector was transfected into H9c2 cells by a cationic reagent, Effecten (QIAGEN, Valencia, CA, U.S.A.), according to the manufacture's protocol. Forty-eight hours after transfection, cells were lysed for evaluation of luciferase activity.

## Western Blot Analysis

Cells were harvested from dishes by scraping, were washed with phosphate-buffered saline, and cell lysates were mixed with sample buffer. The samples were fractionated by sodium dodecyl sulfate-polyacrylamide gel electrophoresis and transferred onto membranes (Millipore Corp., Bedford, MA, U.S.A.). After transfer into the membrane, they were soaked in blocking buffer. The membranes were incubated with a monoclonal phosphor-5′-AMP-activated protein kinase-α (Thr172) antibody (1:1000; Cell Signaling Technology, Beverly, MA, U.S.A.). After the membranes were washed, horseradish peroxidase-conjugated secondary antibodies (Promega, Madison, WI, U.S.A.) were applied and the signal was detected using an enhanced chemi-luminescence system (Amersham, Piscataway, NJ, U.S.A.).

# RESULTS

## Electrical Stimulation Affects Gene Expression of Rat Cardiomyocytes

To investigate transcriptional regulation of cardiomyocytes, primary cultured cardiomyocytes were subjected to ES. Even with a bi-directional current, cardiomyocytes could not be cultured for ES more than 16 hours. As demonstrated in Fig. 1, ES remarkably decreased gene expression of preproET-1 and HIF-1α in the cardiomyocytes, compared with non-stimulated cardiomyocytes. However, the mRNA level of β-actin was not decreased by ES. Adversely, gene expression of glucose transporter 3 mRNA was increased by ES. These results suggested that

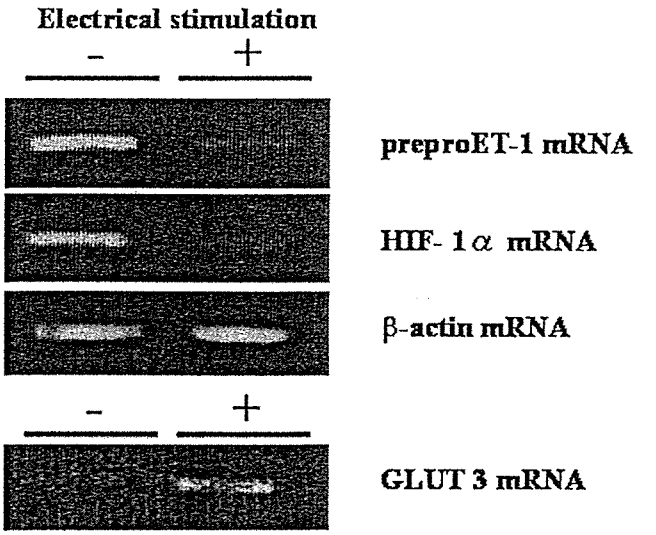


**FIGURE 1.** Electrical stimulation (ES) modifies gene expression of preproendothelin-1 (preproET-1), hypoxia-inducible factor-1α (HIF-1α), and glucose transporter (GLUT) 3 mRNAs. PreproET-1 and HIF-1α gene expressions were decreased 5 hours after ES. In contrast, GLUT 3 gene expression was increased by ES. The level of β-actin mRNA was not affected by ES.

cardiomyocytes respond to ES with an increased gene expression of glucose transporter 3; however, in contrast, such an ES modified gene expression of cardiac preproET-1 and HIF-1α.

## Electrical Stimulation Transcriptionally Regulates PreproET-1 Gene Expression

Further to investigate especially the gene expression of preproET-1 mRNA, a reporter assay was performed using a reporter vector possessing the 5′-promoter regulatory region of the preproET-1 gene. H9c2 cells, a cell line of rat ventricular cardiomyocytes, were transfected by the reporter vector. As shown in Fig. 2, ES of H9c2 cells greatly decreased the luciferase activity of preproET-1. The phenomenon of the depressed luciferase activity was compatible with the decreased preproET-1 mRNA by reverse transcription-PCR.

## Electrical Stimulation Elevates Phosphorylation of 5′-AMP-activated Protein Kinase

To investigate mechanisms to decrease a transcriptional level of preproET-1, we studied whether ES activates the phosphorylation of 5′-AMP-activated protein kinase (AMPK) using H9c2 cells. The time course study demonstrated that AMPK phosphorylation was detected soon after ES (Fig. 3). Furthermore, such an increase in AMPK phosphorylation was also observed in primary cultured cardiomyocytes. It was suggested that ES causes activation of

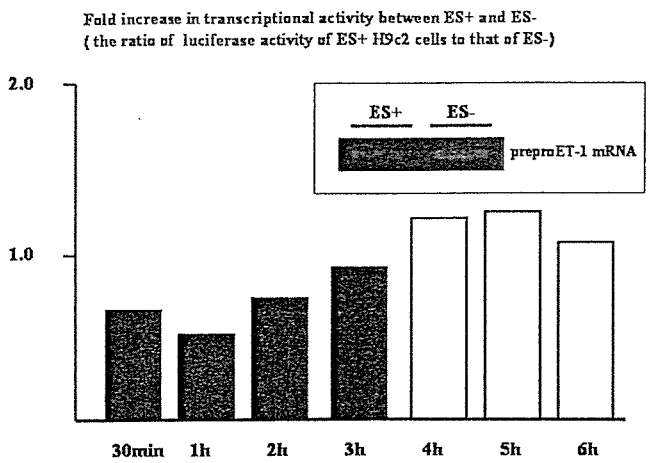


FIGURE 2. Electrical stimulation (ES) transcriptionally represses preproendothelin-1 (preproET-1) gene expression in H9c2 cells. Gene expression of preproET-1 in H9c2 cells was also decreased by ES. Using a reporter vector of the preproET-1 gene, luciferase activity was compared between electrical stimulated (ES+) H9c2 cells and non-electrical stimulated (ES–) cells. The ratio of luciferase activity of ES+ to that of ES– was measured, where a ratio > 1 suggests transcriptional activation, contrasting with a ratio < 1 suggesting repression.

AMPK with a comparable time course of suppression of the preproET-1 gene, and consequently that AMPK phosphorylation is profoundly related to the repression of transcriptional activity of preproET-1 gene expression.

## An Activator of AMPK Causes a Decrease in PreproET-1 mRNA

H9c2 cells were treated by AICAR, which is known as an activator of AMPK. As demonstrated in Fig. 3, AICAR increased the phosphorylation of AMPK. The activation of AMPK occurred very rapidly with a comparable time course of ES. With treatment of AICAR, the mRNA level of preproET-1 was decreased (Fig. 4). It was suggested that AMPK activation was involved in the attenuated preproET-1mRNA gene expression.

## DISCUSSION

ET-1 is one of the aggravating factors in heart failure, because ET-1 further activates the glycolytic system in the failing cardiomyocytes, resulting in aggravation of malfunction in the heart. Therefore, one of the therapeutic goals that inhibit the progression of heart failure might be to decrease cardiac ET-1 gene expression. There are many manipulations to decrease ET-1 gene expression, including blocking the renin–angiotensin system and ET receptor antagonists.[4] However, we have further investigated whether other manipulations can modify the cardiac ET-1 expression,

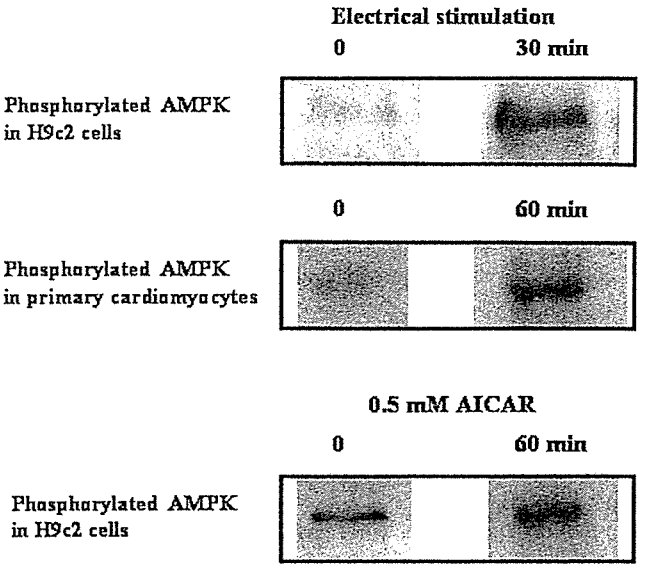


FIGURE 3. 5′-AMP-activated protein kinase (AMPK) is activated through phosphorylation by electrical stimulation (ES). ES caused activation of AMPK through phosphorylation in H9c2 cells. This phenomenon was also detected in rat primary cultured cardiomyocytes with a comparable time course. Also, 0.5 m*M* 5-aminoimidazole-4-carboxamide-1-β-D-ribofuranosyl 5-monophosphate (AICAR), an activator of AMPK, phosphorylated AMPK.

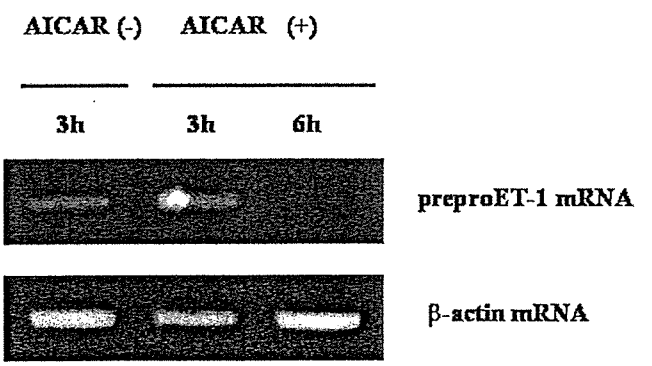


FIGURE 4.. 5′-AMP-activated protein kinase activator decreases preproendothelin-1 (preproET-1) gene expression in H9c2 cells. 5-Aminoimidazole-4-carboxamide-1-β-D-ribofuranosyl 5-monophosphate (AICAR) 1.5 m*M* treatment remarkably decreased the gene expression of preproET-1 mRNA in H9c2 cells.

and then finally we have identified that a mechanical stimulation (i.e. ES) decreases cardiac ET-1 expression through activation of AMPK.

AMPK is known as a fuel sensor kinase, which is activated through phosphorylation when a cellular adenosine triphosphate (ATP) level is decreased.[5] Consequently, cells respond to a shortage of the energy and activate the

phosphorylation of AMPK. This kinase is therefore activated in the early phase to stimuli that might cause mitochondrial dysfunction, leading to ATP deprivation. This response through AMPK phosphorylation is considered an adaptation of cells to avoid cellular death with a shortage of ATP. However, this response is not only involved in pathological states, but also in physiological states. For example, exercise-induced muscle hypertrophy leads to remarkable adaptation of the muscle to the more efficient utilization of energy (i.e. mitochondrial β-oxidation of fatty acid), and consequently to activation of the mitochondrial function.[6] In the case of exercise, AMPK in skeletal muscle is known to be activated.[7] Therefore, it is suggested that the activation of AMPK through phosphorylation is followed by enhancement of mitochondrial function in a physiological condition to obtain more adequate ATP.

It is known that the cardiomyocytes obtain ATP predominantly through mitochondrial β-oxidation of fatty acid; however, when cardiomyocytes were treated by hypoxia, the cardiac energy metabolic system was changed from β-oxidation to glycolysis, because fatty acid oxidation is impaired. In such a case, as our previous study demonstrated, HIF-1α is induced for upregulation of glycolytic enzymes, and furthermore HIF-1α transcriptionally activates preproET-1 gene expression in the failing heart.[2] It is suggested that cardiac ET-1 expression is accompanied with a cellular glycolysis-dominant energy system.[8] With these findings in mind, further speculation is as follows: if the glycolysis-dominant energy system is inhibited, and alternatively mitochondrial β-oxidation of fatty acid is activated, ET-1 gene expression could be decreased. As our present study demonstrated, ES activates the phosphorylation of AMPK in a rapid fashion, followed by a decrease in the transcriptional activity of ET-1.

This is a first demonstration of transcriptional repression of cardiac preproET-1 gene expression using methods other than drugs. Moreover, this reaction is very rapid to decrease preproET-1 mRNA. Therefore, it is suggested that the manipulation of cardiomyocytes by ES is one candidate method to inhibit an increase in cardiac ET-1 gene expression.

## REFERENCES


1. Kakinuma Y, Miyauchi T, Kobayashi T, et al. Myocardial expression of endothelin-2 is altered reciprocally to that of endothelin-1 during ischemia of cardiomyocytes *in vitro* and during heart failure *in vivo*. *Life Sci.* 1999;65:1671–1683.
2. Kakinuma Y, Miyauchi T, Yuki K, et al. Novel molecular mechanism of increased myocardial endothelin-1 expression in the failing heart involving the transcriptional factor hypoxia inducible factor-1α induced for impaired myocardial energy metabolism. *Circulation.* 2001;103: 2387–2394.
3. Kakinuma Y, Miyauchi T, Suzuki T, et al. Enhancement of glycolysis in cardiomyocytes elevates endothelin-1 expression through the transcriptional factor HIF-1α. *Clin Sci.* 2002;103(suppl. 48):210S–214S.
4. Sakai S, Miyauchi T, Kobayashi T, et al. Inhibition of myocardial endothelin pathway improves lomg-term survival in heart failure. *Nature.* 1996;384:353–355.
5. Winder WW. Energy-sensing and signaling by AMP-activated protein kinase in skeletal muscle. *J Appl Physiol.* 2001;91:1017–1028.
6. Saha AK, Schwarsin AJ, Roduit R, et al. Activation of malonyl-CoA decarboxylase in rat skeletal muscle by contraction and the AMP-activated protein kinase activator 5-aminoimidazole-4-carboxamide-1-β-D-ribofuranoside. *J Biol Chem.* 2000;275:24279–24283.
7. Hood DA. Plasticity in skeletal, cardiac, and smooth muscle invited review: contractile activity-induced mitochondrial biogenesis in skeletal muscle. *J Appl Physiol.* 2001;90:1137–1157.
8. Wu-Wong JR, Berg CE, Kramer D. Endothelin stimulates glucose uptake via activation of endothelin-A receptor in neonatal rat cardiomyocytes. *J Cardiovasc Pharmacol.* 2000;36(5 suppl. 1): S179–S183.

*Am J Physiol Heart Circ Physiol* 287: H2906–H2913, 2004;
doi:10.1152/ajpheart.00035.2004.

# A self-calibrating telemetry system for measurement of ventricular pressure-volume relations in conscious, freely moving rats

**Kazunori Uemura,[1] Toru Kawada,[1] Masaru Sugimachi,[1] Can Zheng,[1,2,3] Koji Kashihara,[1,3] Takayuki Sato,[4] and Kenji Sunagawa[1]**

[1]*Department of Cardiovascular Dynamics, National Cardiovascular Center Research Institute, Suita 565-8565;* [2]*Japan Space Forum, Tokyo 105-0013;* [3]*Organization of Pharmaceutical Safety and Research, Tokyo 100-0013; and* [4]*Department of Cardiovascular Control, Kochi Medical School, Nankoku 783-8505, Japan*

Submitted 15 January 2004; accepted in final form 28 July 2004

**Uemura, Kazunori, Toru Kawada, Masaru Sugimachi, Can Zheng, Koji Kashihara, Takayuki Sato, and Kenji Sunagawa.** A self-calibrating telemetry system for measurement of ventricular pressure-volume relations in conscious, freely moving rats. *Am J Physiol Heart Circ Physiol* 287: H2906–H2913, 2004; doi:10.1152/ajpheart.00035.2004.—Using Bluetooth wireless technology, we developed an implantable telemetry system for measurement of the left ventricular pressure-volume relation in conscious, freely moving rats. The telemetry system consisted of a pressure-conductance catheter (1.8-Fr) connected to a small (14-g) fully implantable signal transmitter. To make the system fully telemetric, calibrations such as blood resistivity and parallel conductance were also conducted telemetrically. To estimate blood resistivity, we used four electrodes arranged 0.2 mm apart on the pressure-conductance catheter. To estimate parallel conductance, we used a dual-frequency method. We examined the accuracy of calibrations, stroke volume (SV) measurements, and the reproducibility of the telemetry. The blood resistivity estimated telemetrically agreed with that measured using an ex vivo cuvette method ($y = 1.09x - 11.9$, $r^2 = 0.88$, $n = 10$). Parallel conductance estimated by the dual-frequency (2 and 20 kHz) method correlated well with that measured by a conventional saline injection method ($y = 1.59x - 1.77$, $r^2 = 0.87$, $n = 13$). The telemetric SV closely correlated with the flowmetric SV during inferior vena cava occlusions ($y = 0.96x + 7.5$, $r^2 = 0.96$, $n = 4$). In six conscious rats, differences between the repeated telemetries on different days (3 days apart on average) were reasonably small: 13% for end-diastolic volume, 20% for end-systolic volume, 28% for end-diastolic pressure, and 6% for end-systolic pressure. We conclude that the developed telemetry system enables us to estimate the pressure-volume relation with reasonable accuracy and reproducibility in conscious, untethered rats.

conductance catheter; serial reproducibility; volumetric accuracy; dual-frequency method; Bluetooth

SMALL EXPERIMENTAL ANIMALS, such as rats and mice, are widely used in cardiovascular research. These animals can offer a variety of disease models, including heart failure and hypertension, and enable us to analyze the molecular mechanisms of the pathophysiology underlying such diseases (5, 7, 12, 21, 27). To interpret the molecular findings in terms of cardiac phenotype, an accurate assessment of cardiac function, including the contractile properties of the left ventricle (LV), is required. As a load-insensitive index of LV contractility, the end-systolic pressure-volume relation (ESPVR) has been estimated in small animal species with the use of a conductance catheter technique or an ultrasonic crystal method in acute experimental settings (6, 9, 14, 15, 23). However, the anesthesia and thoracotomy required by these techniques inevitably exert adverse effects on the heart (13, 22, 30). In addition, the time course of disease progression or long-term drug effects cannot be assessed in acute experimental settings (7, 16). To overcome these problems, long-term experimental settings should be developed where the LV pressure-volume relation can be measured telemetrically in small experimental animals.

In the present study, we have developed a new telemetry system to measure LV volume, pressure, and electrocardiogram (ECG) in conscious, freely moving rats. In this system, the LV pressure-volume relation was obtained from a pressure-conductance catheter chronically implanted in the rat LV. To calibrate the conductance signal and obtain absolute LV volume, measurements of blood resistivity ($\rho$) and parallel conductance ($G_p$) are required (3, 4). These calibration procedures require blood sampling and hypertonic saline infusion, but such ex vivo procedures are not applicable to conscious, freely moving small animals. To circumvent such ex vivo procedures in our new telemetry system (29), we adopted a self-calibrating method for the LV volume measurement, as reported in our previous study (28). The aim of the present study was therefore to develop a telemetry system and evaluate its performance. Our results indicate that we succeeded in measuring the LV pressure-volume relation in conscious, untethered rats with reasonable accuracy and reproducibility.

## METHODS

### *Implantable Pressure-Volume Telemetry System*

Figure 1*A* illustrates a newly developed pressure-volume telemetry system for rats; it consists of a pressure-conductance catheter, an analog processor-transmitter (weight = 14 g, volume = 11 ml), and a battery unit (lithium battery; weight = 12 g, volume = 10 ml).

*Pressure-conductance catheter.* Details of the pressure-conductance catheter are presented in Fig. 1*B*. To measure LV conductance, four platinum electrodes (0.25 mm wide) were used. Constant excitation current was applied to the two outermost electrodes while the voltage signal associated with LV conductance was measured from the two inner sensing electrodes. To measure LV pressure, a high-fidelity pressure transducer (Millar Instruments, Houston, TX) was mounted between the two sensing electrodes for the LV conductance measurement. To measure $\rho$, four smaller platinum electrodes (0.1 mm wide, 0.2 mm between centers of adjacent electrodes, 0.6 mm

Address for reprint requests and other correspondence: K. Uemura, Dept. of Cardiovascular Dynamics, National Cardiovascular Center Research Institute, 5-7-1, Fujishirodai, Suita 565-8565, Japan (E-mail: kuemura@ri.ncvc.go.jp).

The costs of publication of this article were defrayed in part by the payment of page charges. The article must therefore be hereby marked "*advertisement*" in accordance with 18 U.S.C. Section 1734 solely to indicate this fact.

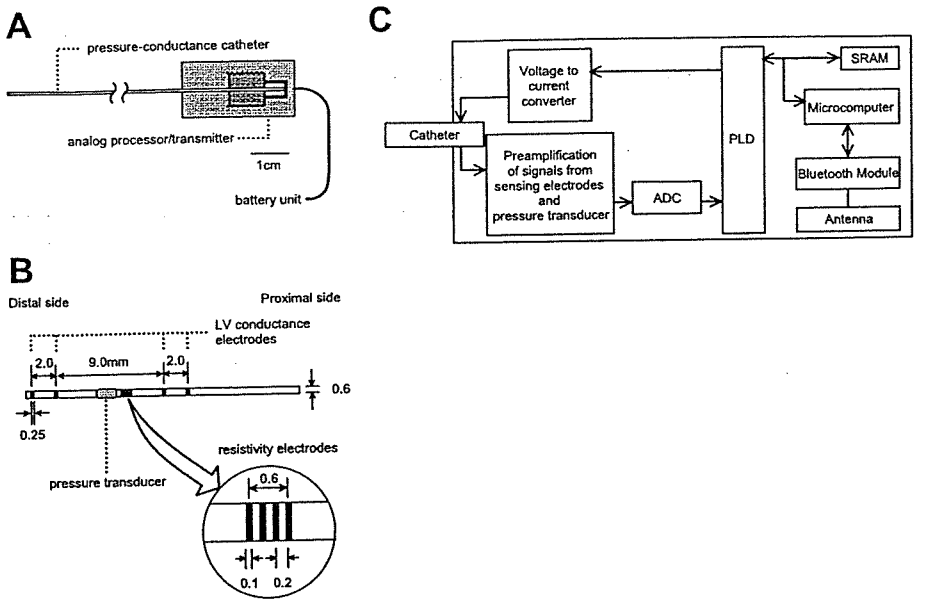


Fig. 1. *A*: schematic illustration of our pressure-volume telemetry system. A 10-cm-long pressure-conductance catheter obtains signals of left ventricular (LV) conductance and pressure, intraventricular blood resistivity, and an ECG. Signals are processed and transmitted by an analog processor transmitter, which is powered by a battery unit (lithium battery). *B*: schematic illustration of our pressure-conductance catheter. Catheter has 4 electrodes for measurement of LV conductance and 4 electrodes for measurement of intraventricular blood resistivity (*inset*). A high-fidelity pressure transducer is mounted between *electrodes 2* and *3*. *C*: block diagram of an analog processor transmitter. ADC, analog-to-digital converter; PLD, programmable logic device; SRAM, static random access memory.

between centers of excitation electrodes) were placed near the pressure transducer (Fig. 1*B*, *inset*). Constant excitation current was applied to the two outer electrodes while the voltage signal associated with ρ was measured from the two inner electrodes.

*Analog processor transmitter.* A block diagram of the analog processor transmitter is presented in Fig. 1*C*. It was equipped with several functions. First, it delivered a dual-frequency (2 and 20 kHz) constant excitation current [20 μA root mean square (RMS)] for measurements of LV conductance and ρ. We validated the current output by injecting it into known resistors and examining the developed voltage. The resulting RMS current output was 20.4 μA (SD 0.2) and 19.3 μA (SD 0.2) at 2 and 20 kHz, respectively. These values were constant over different resistors (50–990 Ω). Second, it measured and processed the voltage signal from the sensing electrodes as follows: Analog signals were digitized (12 bits, 40-kHz sampling rate; model ADS7870, Texas Instruments, Dallas, TX) and then fed into a programmable logic device (model XC 2C256, Xilinx, San Jose, CA), which processed them to yield RMS digital signals corresponding to frequency components of 2 and 20 kHz and a low-frequency signal (<2 kHz; see APPENDIX). The circuit was connected to the larger or smaller electrodes in response to a command signal, so that LV conductance or ρ could be measured. Third, the analog processor-transmitter had a bridge amplifier for the LV pressure measurement. The LV pressure signal was also digitized (12 bits, 40-kHz sampling rate). All these functions were controlled by a microcomputer (model H8S, Hitachi, Tokyo, Japan).

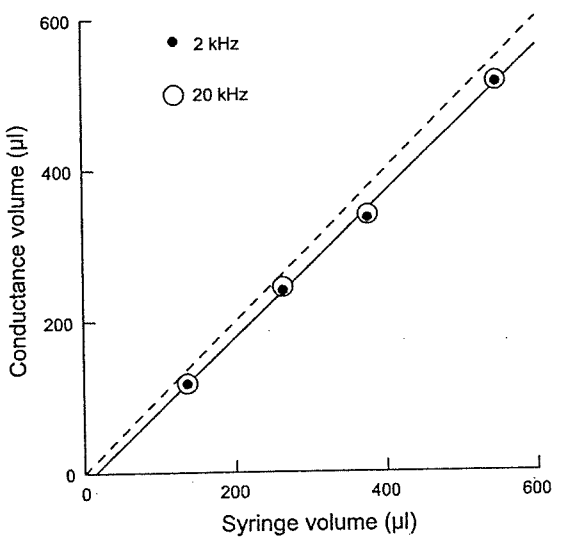


Fig. 2. Comparison of conductance-derived volumes at 2 and 20 kHz vs. known fluid volumes of syringes. Both conductance-derived volumes were essentially identical for each of the syringe volumes. Relation between conductance-derived volume and syringe volume was quite linear. Solid line, regression between conductance-derived volume at 20 kHz and syringe volume; dashed line, identity.

Bluetooth technology was used to transmit the data (18). For real-time monitoring, all processed signals were resampled at 200 Hz by the microcomputer and transmitted to an external receiver (CASIRA, CSR, Cambridge, UK) by a Bluetooth module (model LMBTB027, Murata, Tokyo, Japan). For high-precision non-real-time analysis, signals recorded at 2,000 Hz over a 6-s interval were stored in a static random access memory (model HM62V16256, Hitachi) and then transmitted to the receiver by the Bluetooth module. The external receiver detected the radio-frequency signal from the transmitter and converted it to a serial bit stream.

### *Self-Calibration of Ventricular Volumetry*

The principles of conductance volumetry have been described previously (3, 4). Briefly, the ventricular conductance signal ($G$) can be converted to absolute ventricular volume (V) as follows

$$V = (1/\alpha)\,(L^2 \cdot \rho)\,(G - G_p) \qquad (1)$$

where α is a volume calibration factor, $L$ is the distance between the sensing electrodes, ρ is blood resistivity, and $G_p$ is parallel conductance. $L$ was 9 mm in the present catheter design.

In a preliminary experiment, when the catheter was placed in a series of graduated syringes filled with diluted saline, conductance-derived volumes at 2 and 20 kHz were close to the true syringe volume in the volume range of interest (Fig. 2). Conductance-derived volumes at the two frequencies were essentially identical for each of the syringe volumes. Hence, α was assumed to be unity in the present study (14, 23).

The four smaller electrodes were used to estimate ρ (Fig. 1*B*, *inset*). The distance between the excitation electrodes was set at 0.6 mm. In an in vitro experiment, we confirmed that the current distribution volume was confined to an ~4-mm diameter around the catheter with this electrode design (see APPENDIX). The end-diastolic LV diameter is 7–9 mm in normal rats and 9–12 mm in rats with left heart failure (17). Because the interelectrode distance between the excitation electrodes was small enough to confine the current distribution volume to within the end-diastolic ventricular blood pool in the rat LV, we estimated ρ at end diastole (10, 28).

$G_p$ was estimated by the dual-frequency excitation method (8, 9, 28) as follows

$$G_p = \kappa \times \Delta G_{20-2} \quad (2)$$

where $\Delta G_{20-2}$ is the difference in ventricular conductance values between the 20- and 2-kHz excitation frequencies and κ is an experimentally derived constant. Once κ is determined, $G_p$ can be estimated from $\Delta G_{20-2}$, obviating the need for saline infusion.

*Instrumentation and Experimental Protocols*

Thirty-three male Sprague-Dawley rats (350–400 g body wt) were used. Care of the animals was in strict accordance with the *Guiding Principles for the Care and Use of Animals in the Field of Physiological Sciences* as approved by the Physiological Society of Japan. The animals were anesthetized with pentobarbital sodium (50 mg/kg ip) and ventilated artificially. A vertical midline cervical incision was made to expose the right common carotid artery while the animal was in the supine position. The pressure-conductance catheter of the telemetry system was inserted into the LV retrogradely from the right common carotid artery. The position of the catheter was verified by monitoring the pressure-volume signal and by two-dimensional echocardiography. At the conclusion of the experiment, the animal was killed with an overdose of pentobarbital sodium, and the heart was examined to reconfirm the proper positioning of the catheter.

*Group 1 (n = 23).* We evaluated the accuracy of telemetric calibration of ρ and $G_p$ under anesthetized, closed-chest conditions. Catheters (3-Fr) were inserted into the right and left jugular veins for blood sampling and saline injection, respectively. In 10 of the 23 rats, we compared ρ estimated telemetrically ($\rho_{est}$) with ρ measured from sampled blood by a conventional ex vivo cuvette method ($\rho_{conv}$). In the remaining 13 rats, we estimated $G_p$ by the dual-frequency excitation method ($G_{p,est}$) and by the hypertonic saline method ($G_{p,conv}$). To obtain $G_{p,conv}$, we injected 20 μl of saturated saline into the right jugular vein while continuously measuring LV conductance (14, 23). To obtain $G_{p,est}$, we measured LV conductance at 2- and 20-kHz excitation frequencies and derived $\Delta G_{20-2}$ by averaging the instantaneous conductance difference over ~10 cardiac cycles. We randomly selected 7 of the 13 rats and determined the proportionality constant (κ in *Eq. 2*) from the averaged ratio of $G_{p,conv}$ to $\Delta G_{20-2}$. $G_{p,est}$ and $G_{p,conv}$ were measured while the artificial ventilation was temporarily suspended at end expiration.

*Group 2 (n = 4).* Under anesthetized, open-chest conditions, we evaluated the accuracy of volumetry by comparing stroke volume (SV) measured by the telemetry system with SV measured by an ultrasonic flowmeter (model 2.5S273, Transonic Systems, Ithaca, NY). After median sternotomy, the aortic arch was dissected free from surrounding tissues. A flow probe was placed around the ascending aorta to measure the aortic blood flow. A string occluder was placed loosely around the inferior vena cava to decrease the LV preload and vary the SV over a wide range. We simultaneously measured the telemetric LV volume and the ultrasonic aortic blood flow while varying the preload. The measurements were done while the artificial ventilation was temporarily suspended at end expiration.

*Group 3 (n = 6).* Under conscious, closed-chest conditions, we evaluated the reproducibility of the telemetry on different days. Aseptic conditions were maintained throughout the surgical procedure. The telemetry system was implanted in a subcutaneous pocket made at the right upper dorsum. The skin was closed, and the animal was allowed to recover from anesthesia. On the day after implantation surgery, the LV volume, pressure, and an ECG were measured telemetrically in the fully recovered, conscious animal (*study 1*). Each rat underwent a second set of telemetric measurements at 1–6 days after the initial study (*study 2*). Ambient barometric pressure was measured simultaneously and subtracted from the telemetric LV pressure to compensate for changes in atmospheric pressure.

*Data Collection*

We used the real-time mode (200-Hz sampling) of the telemetry system and recorded LV conductance, LV pressure, intraventricular ECG, and ρ on a hard disk of a dedicated laboratory computer system (model HFPA031003, Epson, Tokyo, Japan). In *group 2*, ultrasonic aortic blood flow was digitized at 1,000 Hz through a 12-bit analog-to-digital converter and stored on a hard disk for subsequent analyses.

*Statistical Analysis*

For the calculation of LV volume using *Eq. 1*, *G* and ρ were obtained from the 20-kHz frequency component. In *group 1*, we used linear regression analysis to compare the telemetric and conventional measurements of ρ ($\rho_{est}$ vs. $\rho_{conv}$) and $G_p$ ($G_{p,est}$ vs. $G_{p,conv}$). In *group 2*, we calculated the telemetric SV from the difference between the end-diastolic volume (EDV) and end-systolic volume (ESV) in each beat. The flowmetric SV was computed from the time integral of aortic blood flow. The telemetric SV was compared with the flowmetric SV by linear regression analysis. In *group 3*, we compared heart rate (HR), EDV, ESV, end-diastolic pressure (EDP), and end-systolic pressure (ESP) between *study 1* and *study 2* for each rat. Using the pressure-volume data, we calculated ejection fraction (EF), maximal pressure increase ($+dP/dt_{max}$) or decrease ($-dP/dt_{max}$) over time, and the time constant of isovolumic relaxation (τ) and compared them between *study 1* and *study 2* for each rat. A nonparametric multiple comparison (Wilcoxon's signed-rank test) was used to examine the difference in each parameter between *study 1* and *study 2*. Group data are expressed as means (SD). Differences were considered significant at $P < 0.05$.

## RESULTS

*Telemetric Calibration of ρ*

Figure 3*A* is a representative time series showing LV pressure and ρ at 2 and 20 kHz derived from the telemetry. The bottom of the ρ waveform, which corresponded to end diastole, represents the time when there was sufficient blood volume around the catheter (10). The lowest ρ values at 2 kHz ($\rho_{2\,kHz}$) and 20 kHz ($\rho_{20\,kHz}$) were very close (197 and 207 Ω·cm, respectively). This was the case for all the rats, indicating that ρ was frequency independent ($\rho_{2\,kHz} = 1.08\rho_{20\,kHz} - 13.8$, $r^2 = 0.96$, SE of the estimate = 6.7 Ω·cm) (6, 9). The lowest ρ at 20 kHz was treated as $\rho_{est}$.

Figure 3*B* summarizes the relation between $\rho_{est}$ and $\rho_{conv}$ obtained from 10 rats in *group 1*. $\rho_{est}$ agreed with $\rho_{conv}$ reasonably well ($\rho_{est} = 1.09\rho_{conv} - 11.9$, $r^2 = 0.88$, SE of the estimate = 10.7 Ω·cm). The ratio of SE of the estimate to the mean of $\rho_{est}$ was 0.046, indicating small variability around the regression line.

*Telemetric Calibration of $G_p$*

Figure 4*A* illustrates a representative time series of telemetrically measured ECG, LV conductance signals at 2 and 20 kHz, and LV pressure. In this animal, $\Delta G_{20-2}$ was 0.56 mS

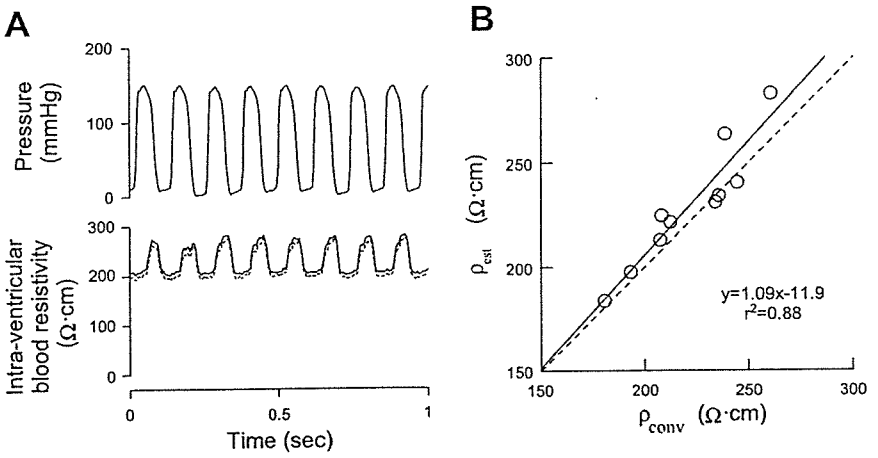


Fig. 3. *A*: waveforms of ventricular pressure and intraventricular blood resistivity at 2 kHz (dashed line) and 20 kHz (solid line) as a function of time obtained telemetrically. *B*: relation between blood resistivity as measured in a cuvette ($\rho_{conv}$) and as estimated via catheter electrodes ($\rho_{est}$) in 10 rats. Solid line, regression; dashed line, identity.

and $G_{p,conv}$ was 3.27 mS. Therefore, $\kappa$ was calculated to be 5.79 from *Eq. 2* in this animal. The averaged $\kappa$ from seven randomly selected rats was 5.14, which we used as the experimentally derived constant to obtain $G_{p,est}$ for all rats.

Figure 4*B* summarizes the relation between $G_{p,est}$ and $G_{p,conv}$ obtained from 13 rats in *group 1*. $G_{p,est}$ correlated well with $G_{p,conv}$ ($G_{p,est} = 1.59G_{p,conv} - 1.77$, $r^2 = 0.87$, SE of the estimate = 0.33 mS). The ratio of SE of the estimate to the mean of $G_{p,est}$ was 0.11, indicating that the estimation was reasonable around the mean of $G_{p,est}$.

*Accuracy of the Televolumetry*

Figure 5*A* depicts LV pressure and volume measured by telemetry and aortic blood flow measured by the ultrasonic flowmeter. Vena caval occlusion decreased LV pressure, volume, and aortic blood flow.

Figure 5*B* summarizes the relation between telemetric SV ($SV_{tele}$) and flowmetric SV ($SV_{flow}$) obtained from four rats in *group 2*. $SV_{tele}$ matched $SV_{flow}$ reasonably well in each of the four rats: $r^2 = 0.90-0.99$, slope = 0.86 (SD 0.16), intercept = 12.4 μl (SD 10.4), and SE of the estimate = 4.3 μl (SD 0.4). A linear regression analysis on the pooled data from all four rats also showed a highly linear relation between $SV_{tele}$ and $SV_{flow}$: $SV_{tele} = 0.96SV_{flow} + 7.5$, $r^2 = 0.96$, SE of the estimate = 6.6 μl. The ratio of SE of the estimate to the mean of $SV_{tele}$ was 0.10.

*Reproducibility of the Telemetry*

Individual data obtained by the telemetry system for all six rats in *group 3* are provided in Tables 1 and 2. The overall variability between repeated measurements in the same rat was reasonably small. There were no significant differences in repeated measurements of HR, EDV, ESV, EDP, and ESP between *study 1* and *study 2* (Table 1). There were no significant differences in repeated measurements of EF, $+dP/dt_{max}$, $-dP/dt_{max}$, and $\tau$ between *study 1* and *study 2* (Table 2).

Figure 6 illustrates the representative LV pressure-volume loops obtained from a rat in *group 3*. The pressure-volume loops in *studies 1* and *2* were almost identical.

## DISCUSSION

We have developed a novel telemetry system for measurements of LV volume, pressure, and ECG in conscious, freely moving rats. The system, for the first time to the best of our knowledge, has enabled measurement of the LV pressure-

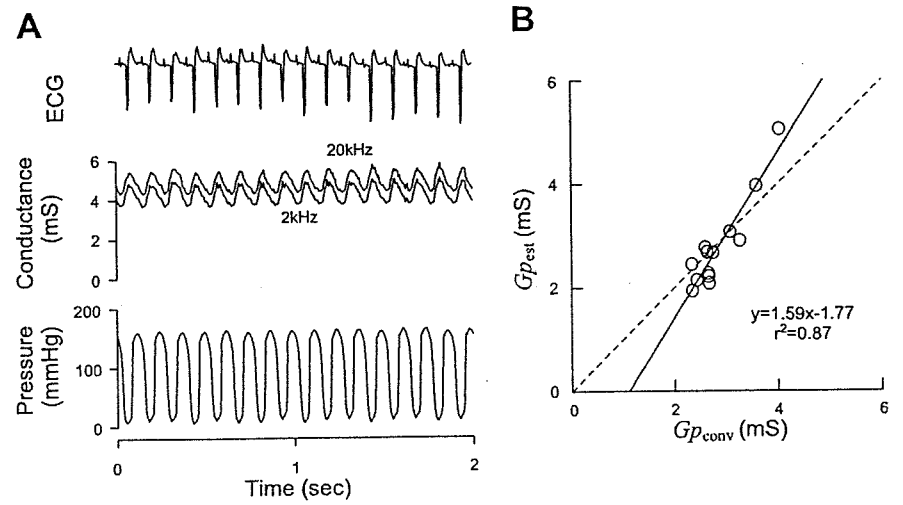


Fig. 4. *A*: waveforms of an ECG, conductance signals at 2 and 20 kHz, and ventricular pressure as a function of time, obtained telemetrically. *B*: relation between parallel conductance estimated by the saline infusion method ($G_{p,conv}$) and by dual-frequency excitation method ($G_{p,est}$) in 13 rats. Solid line, regression; dashed line, identity.

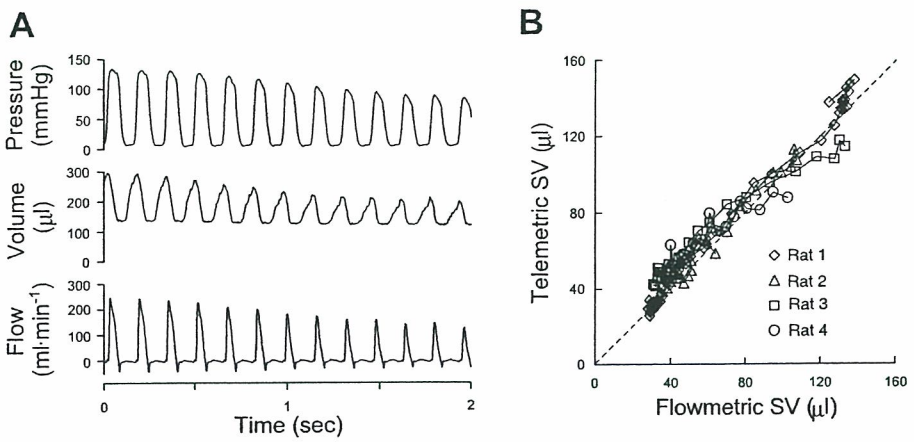


Fig. 5. *A*: representative traces of ventricular pressure, ventricular volume obtained telemetrically, and aortic flow measured by an ultrasonic flowmeter during vena cava occlusion in 1 rat. *B*: relation between telemetric stroke volume (SV) and flowmetric SV in 4 rats. Dashed line, identity.

volume relation in small experimental animals, such as rats, under completely conscious, unrestricted conditions with reasonably good accuracy and reproducibility.

*Self-Calibrating Volumetry*

In our conductance volumetric system, $\rho$ and $G_P$ were estimated using the telemetric signals alone (Figs. 3 and 4). We will be able to use the empirical constant $\kappa$ (=5.14), determined in this study, in the future application of our telemetry system to rats. The self-calibrating feature made it possible to measure the LV pressure-volume relation in rats without tethering them for ex vivo calibration procedures, such as blood sampling and hypertonic saline infusion. Besides their impracticality in conscious, small animals, these procedures can alter hemodynamic conditions (6, 9). Frequent blood sampling can induce anemia. Concentrated saline injection depresses myocardial contractility and has volume-loading effects (6, 9). Our telemetry system is free of these problems.

The current used for resistivity measurements was distributed in a 2-mm radius around the catheter (see APPENDIX). The ratio of the radius (i.e., penetration depth) to the distance between the excitation electrodes was ~3 (≒2/0.6). This ratio is at odds with previously reported values, which were around or less than unity (6, 10, 26). Penetration depth is affected by the relation between the resistivity of the target tissue and that of the surrounding structure (26). This relation in our study was different from those in previous studies, which would be one reason for the discrepancy. Difference in shape and arrangement of the electrodes between our system and those previous studies would be another reason. Because the electrodes were placed very closely, stray capacitance between connecting wires could be a problem (31). The fact that resistivity values at 2 and 20 kHz were very close indicated that our titration method effectively removed the problem of stray capacitance (see APPENDIX). However, it might be better to incorporate techniques such as capacitance neutralization to completely prevent the problem, in case the capacitance were to significantly affect our titration accuracy in future long-term use, e.g., with increases in electrode impedance (31).

We used the dual-frequency excitation method previously described by Gawne et al. (8). Feldman et al. (6) combined measured resistivity of the myocardium with an analytic approach and estimated $G_p$ from the conductance signals at 10 and 100 kHz. Although their method was completely independent of saline injection, it required measurement of myocardial resistivity with an additional four-electrode sensor.

*Volumetric Accuracy and Reproducibility*

We have verified the volumetric accuracy of our telemetry system by comparing $SV_{tele}$ with $SV_{flow}$ during inferior vena cava occlusions (Fig. 5*A*). The volumetric accuracy of the conductance catheter technique in the rat heart has been ex-

Table 1. *Reproducibility of hemodynamic variables*

| | HR, beats/min | | EDV, μl | | ESV, μl | | EDP, mmHg | | ESP, mmHg | |
|---|---|---|---|---|---|---|---|---|---|---|
| Rat | S1 | S2 | S1 | S2 | S1 | S2 | S1 | S2 | S1 | S2 |
| *1* | 530 | 475 | 303 | 307 | 168 | 182 | 14 | 19 | 131 | 123 |
| 2 | 363 | 476 | 310 | 280 | 212 | 151 | 11 | 17 | 121 | 133 |
| *3* | 426 | 500 | 330 | 355 | 212 | 220 | 12 | 9 | 127 | 129 |
| *4* | 405 | 511 | 244 | 194 | 143 | 89 | 14 | 13 | 120 | 125 |
| *5* | 402 | 382 | 364 | 434 | 269 | 326 | 15 | 14 | 119 | 106 |
| *6* | 400 | 380 | 240 | 283 | 158 | 167 | 24 | 36 | 142 | 152 |
| Mean (SD) | 421 (57.3) | 454 (58.2) | 299 (49) | 309 (81) | 194 (47) | 189 (80) | 15 (5) | 18 (10) | 127 (9) | 128 (15) |
| Difference | | | | | | | | | | |
| Mean (SD) | 65 (40) | | 37 (23) | | 34 (26) | | 5 (4) | | 8 (4) | |
| Percent difference | | | | | | | | | | |
| Mean (SD) | 15 (9) | | 13 (8) | | 20 (17) | | 28 (16) | | 6 (4) | |

S1, *study 1;* S2, *study 2;* HR, heart rate; EDV, left ventricular end-diastolic volume; ESV, left ventricular end-systolic volume; EDP, left ventricular end-diastolic pressure; ESP, left ventricular end-systolic pressure.

Table 2. *Reproducibility of parameters of ventricular functions*

| Rat | EF, % | | +dP/dt$_{max}$, mmHg/s | | −dP/dt$_{max}$, mmHg/s | | τ, ms | |
|---|---|---|---|---|---|---|---|---|
| | S1 | S2 | S1 | S2 | S1 | S2 | S1 | S2 |
| *1* | 45 | 41 | 10,594 | 9,615 | 7,165 | 6,648 | 9.2 | 9.0 |
| *2* | 32 | 46 | 9,284 | 11,802 | 6,364 | 7,372 | 8.5 | 8.3 |
| *3* | 36 | 38 | 10,373 | 12,129 | 7,277 | 6,937 | 9.4 | 8.1 |
| *4* | 42 | 54 | 9,274 | 11,801 | 7,527 | 7,013 | 6.4 | 9.5 |
| *5* | 26 | 25 | 8,862 | 7,610 | 6,132 | 4,878 | 7.4 | 7.9 |
| *6* | 34 | 41 | 9,808 | 9,756 | 7,518 | 7,273 | 11.0 | 12.4 |
| Mean (SD) | 36 (7) | 41 (10) | 9,699 (682) | 10,452 (1,773) | 6,997 (601) | 6,687 (923) | 8.7 (1.6) | 9.2 (1.7) |
| Difference | | | | | | | | |
| Mean (SD) | 7 (5) | | 1513 (957) | | 646 (397) | | 1.1 (1.1) | |
| Percent difference | | | | | | | | |
| Mean (SD) | 17 (13) | | 15 (9) | | 10 (7) | | 13 (14) | |

EF, left ventricular ejection fraction; dP/dt$_{max}$, maximal pressure rise (+) or decrease (−) over time; τ, time constant of isovolumic left ventricular relaxation.

amined using a similar comparison (14, 23). Ito et al. (14) reported a very high and linear correlation ($r$ = 0.97–0.99) between conductance-derived SV and SV measured by an electromagnetic flowmeter in rats. We also obtained a similar highly linear relation between $SV_{tele}$ and $SV_{flow}$ (Fig. 5*B*).

The reproducibility of our telemetry system (Table 1) is good enough for many applications, such as the study of LV remodeling in rats. This is because EDV has been reported to increase to ~200% of the control value in rats with ischemic heart failure and in heart failure-prone rats (2, 7, 12).

*Applications of the Telemetry System*

The developed telemetry system enables detailed evaluation of cardiac function in small animals by eliminating the effects of anesthesia and acute surgical intervention (13, 22, 30). By using a single-beat estimation method to determine the ESPVR, our system would enable evaluation of the load-independent contractile index in conscious animals (24, 25). We validated pressure-volume signals only under control conditions in this study. The stability of the acquired data and the capacity of our system to monitor altered hemodynamics remain to be evaluated.

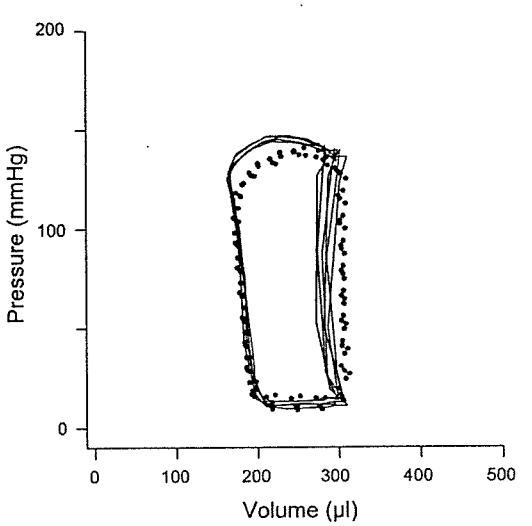


Fig. 6. Day-to-day reproducibility of LV pressure-volume loops in 1 rat. Thick solid loops, *study 1*; dotted loops, *study 2*. Loops for *studies 1* and *2* (6 days apart) were superimposable.

Our telemetry system is potentially useful for the long-term monitoring of LV function. We confirmed that our system was viable for up to 8 days in this study. However, further studies are required to definitively evaluate the longevity of the implants over a longer period of time (19). Thrombosis and infection would affect the morbidity and mortality associated with the chronic implantation of our system. Coating of the pressure-conductance catheter with anticoagulants and further miniaturization of the implant are under development to ameliorate such problems.

We adopted Bluetooth technology for telecommunication. Bluetooth is a wireless technology designed to allow low-cost, short-range radio links between mobile personal computers and other portable devices (18). While point-to-point connections are supported, Bluetooth technology allows up to seven simultaneous connections to be established and maintained by a single receiver (18). This unique feature of Bluetooth technology should be beneficial in experimental settings where a large population of animals in a single cage must be evaluated (16).

*Limitations*

The volume calibration factor α was assumed to be unity on the basis of the preliminary experiment, where the conductance-derived volume was close to true syringe volume in the normal operating range for rats (Fig. 2). Georgakopoulos and Kass (9) noted that the relation was quite linear when the volume range was limited to the physiological operating range for mice. Hettrick et al. (11) also noted that conductance-derived volume was close to true syringe volume and α was unity in a volume range. However, both groups and others noted that the relation was nonlinear when considered over a wider volume range (1, 9, 11, 20). In addition, the syringes have no $G_p$, whereas the rat heart does. It has been shown that $G_p$ has significant effects on α (11). Taken together, these findings suggest that it will be necessary to recalibrate α when we apply our system to the rat LV in heart failure or other cardiac disorders, where drastic changes in ventricular volume and changes in the electrical properties of surrounding structures, i.e., change in $G_p$, are probable (1).

Values of EF in Table 2 are low for normal rats (5, 7). Other parameters of LV function are, however, within the normal